CONFIDENTIAL

Copy 311

RM A53J07

NACA RM A53J07

NACA

RESEARCH MEMORANDUM

THE EFFECTS OF HORIZONTAL-TAIL HEIGHT AND A PARTIAL-SPAN LEADING-EDGE EXTENSION ON THE STATIC LONGITUDINAL STABILITY OF A WING-FUSELAGE-TAIL COMBINATION HAVING A SWEPTBACK WING

By Angelo Bandettini and Ralph Selan

Ames Aeronautical Laboratory
Moffett Field, Calif.

CLASSIFICATION CHANGED TO UNCLASSIFIED
AUTHORITY: J.W. CROWLEY DATE: 10-14-55
CHANGE NO. 3140
WHL

CLASSIFIED DOCUMENT

This material contains information affecting the National Defense of the United States within the meaning of the espionage laws, Title 18, U.S.C., Secs. 793 and 794, the transmission or revelation of which in any manner to an unauthorized person is prohibited by law.

NATIONAL ADVISORY COMMITTEE FOR AERONAUTICS

WASHINGTON

March 9, 1954

CONFIDENTIAL

NATIONAL ADVISORY COMMITTEE FOR AERONAUTICS

RESEARCH MEMORANDUM

THE EFFECTS OF HORIZONTAL-TAIL HEIGHT AND A PARTIAL-SPAN LEADING-EDGE EXTENSION ON THE STATIC LONGITUDINAL STABILITY OF A WING-FUSELAGE-TAIL COMBINATION HAVING A SWEPTBACK WING

By Angelo Bandettini and Ralph Selan

SUMMARY

An investigation has been made to evaluate the effects of vertical height of the horizontal tail on the static longitudinal stability of a model having a wing with 35° of sweepback, an aspect ratio of 4.5, a taper ratio of 0.5, and NACA 64A010 sections. The investigation also included the effects of adding a partial-span, leading-edge chord extension to the outer portions of the wing. The tests were made in the Ames 12-foot pressure wind tunnel at a constant Reynolds number of 2,000,000 and Mach numbers up to 0.92. At a Mach number of 0.20, tests were also made at a Reynolds number of 11,000,000.

Results of tests of the model with the tail in the high position indicated large forward movements of the center of pressure at moderate lift coefficients for Mach numbers below 0.92. Lowering the horizontal tail was effective in improving the stability by reducing a loss in tail effectiveness at the high lift coefficients for all Mach numbers below 0.90. Effective downwash at the tail computed from the force and moment data and wing-wake surveys indicated that the improved stability with the low tail resulted from more favorable downwash characteristics at the high angles of attack.

Addition of the leading-edge extension to the wing with the tail in the low position eliminated the forward movement of center of pressure at moderate lift coefficients for all Mach numbers below 0.90. At Mach numbers of 0.90 and 0.92, addition of the leading-edge extension resulted in only minor changes in the stability.

INTRODUCTION

Adverse variations in the longitudinal stability of swept-wing airplanes during certain phases of flight produce objectionable flying characteristics that have been the subject of considerable study during the past few years. Some of the stability variations have been eliminated or considerably reduced by the use of stall control devices, but other unsatisfactory longitudinal stability characteristics, particularly those occurring at high subsonic Mach numbers, have not been amenable to improvement by use of such devices. One airplane which has typical longitudinal instability at high speed and moderate lift coefficients was the subject of flight investigations (refs. 1, 2, and 3) which indicated that modifications to the wing, such as the addition of vortex generators or fences, did not produce adequate improvements in the stability. An investigation in the Ames 12-foot pressure wind tunnel of a model with a wing similar in plan form to that of this airplane also indicated that addition of a fence and leading-edge chord extensions do not result in satisfactory stability, since they failed to eliminate a forward movement of the center of pressure at the higher angles of attack at Mach numbers above 0.85 (see ref. 4).

Although the objectionable stability changes apparent from the data in reference 4 were attributable primarily to the pitching-moment characteristics of the wing-fuselage combination, they were aggravated by variations in the contribution of the tail to stability, indicating that an improvement might be realized by locating the tail in a region where downwash distribution or wake effects would be more favorable.

Wind-tunnel tests of various models with swept wings, such as those reported in references 5, 6, and 7, have indicated that the tail contribution to stability at high angles of attack could be increased substantially by locating the tail near the wing chord plane extended. The model described in reference 4 had the tail 22 percent of the wing semispan above the wing chord plane extended, which corresponded to the tail position of the swept-wing airplane that was the subject of flight tests reported in reference 1. For the investigation described in the present report, the same model was tested in the Ames 12-foot wind tunnel with the tail in a low position, 8-percent semispan above the wing chord plane extended. This position was selected in order to duplicate the location of the horizontal tail of an airplane (similar to the one previously mentioned) which was modified for flight tests with the tail at the bottom of the fuselage.

The results described in this report include wake surveys at the tail as well as the evaluation of the effective wing downwash at the two tail locations. In addition, the effect of adding one of the

leading-edge chord extensions employed in the tests reported in reference 4 was investigated on the model with the tail in the low position.

NOTATION

All areas and dimensions used in the following symbols refer to the unmodified wing:

b wing span

c local wing chord parallel to the plane of symmetry

c_{av} average chord, $\frac{2S}{b}$

C_l section lift coefficient

$\bar{c}$ wing mean aerodynamic chord, $\frac{\int_0^{b/2} c^2 dy}{\int_0^{b/2} c\, dy}$

C_D drag coefficient, $\frac{\text{drag}}{qS_w}$

C_L lift coefficient, $\frac{\text{lift}}{qS_w}$

C_m pitching-moment coefficient about the quarter-point of the wing mean aerodynamic chord, $\frac{\text{pitching moment}}{qS_w\bar{c}}$

i_t incidence of the horizontal tail measured from body center line, negative when trailing edge is up, deg

l length of body

l_t tail length, distance from the quarter-point of the wing mean aerodynamic chord to the quarter-point of the horizontal-tail mean aerodynamic chord

M free-stream Mach number

q free-stream dynamic pressure

R Reynolds number based on wing mean aerodynamic chord

r local radius of body

r_o maximum radius of body

S area of semispan wing

V_t horizontal-tail volume, $\frac{S_t\ l_t}{S_w \bar{c}}$

x coordinate in the longitudinal direction, parallel to the plane of symmetry

y coordinate in the lateral direction, normal to the plane of symmetry

z coordinate in the vertical direction, parallel to the plane of symmetry

α angle of attack measured from body center line, deg

ϵ downwash angle, deg

$\left(\frac{dC_m}{dC_L}\right)_t$ tail stability parameter, $-\left[\frac{(dC_L/d\alpha)_t}{(dC_L/d\alpha)_{w+b}}\left(\eta\frac{q_t}{q}\right)V_t\left(1-\frac{d\epsilon}{d\alpha}\right)\right]$

$\left(\frac{dC_L}{d\alpha}\right)$ lift-curve slope, per deg

$\left(\frac{\partial C_m}{\partial i_t}\right)$ tail-control effectiveness parameter, measured at a constant angle of attack

$\eta\left(\frac{q_t}{q}\right)$ tail efficiency factor (ratio of the lift-curve slope of the horizontal tail when mounted on the fuselage in the flow field of the wing to the lift-curve slope of the isolated horizontal tail)

Subscripts

b body

t horizontal tail

w wing

MODEL DESCRIPTION

The geometry of the model is shown in figure 1 and in table I. A photograph of the complete model with the tail in the high position is shown in figure 2(a). Details of the construction of the wing, leading-edge extension, body, and tail have been discussed in reference 4.

The basic wing had the quarter-chord line swept back 35°, an aspect ratio of 4.5, and a taper ratio of 0.5. The wing sections in planes perpendicular to the quarter-chord line were the NACA 64A010. The leading-edge chord extension occupied the outer 42 percent of the wing semispan (figs. 1 and 2(b)). The coordinates of a section with the 15-percent-chord leading-edge extension are shown in table II of reference 4.

The horizontal tail was not swept and had an aspect ratio of 4.3 and a taper ratio of 1.0. The sections of the tail were the NACA 63A004. The tail height is defined as the perpendicular distance between the wing chord plane extended and the 0.25 c point of the tail (fig. 1). In this investigation, the tail position equal to 22 percent of the semispan above the extended wing chord plane is referred to as the high tail position (figs. 1 and 2(c)) and the tail position 8 percent of the semispan above the extended wing chord plane is referred to as the low tail position (figs. 1 and 2(d)). For both the high and the low tail positions, the horizontal-tail surface was supported above the fuselage center line by a vertical steel strut. The juncture between the strut and the tail surface in each case was enclosed by streamlined fairings made of mahogany (figs. 2(c) and 2(d)). The incidence of the tail is referred to the body center line and was changed by rotation about the 0.50 c point of the tail.

The air-stream survey rake was mounted on an extension of the body spar at approximately the same location as the tail (figs. 2(e) and 2(f)). The stagnation pressures were measured by 25 tubes on each of three rakes, each rake being located at a different spanwise station. The static pressure at the tail was assumed equal to the free-stream static pressure. The downwash angles were also measured at three spanwise

stations. The longitudinal, vertical, and spanwise positions of the tubes in the survey rake are given in table I. The wake was surveyed in a plane 0.14 c_t behind the leading edge of the tail and the downwash angles were measured 0.7 c_t ahead of the leading edge of the tail.

TESTS

Measurements of lift, drag, and pitching moment were made for the model and its components in the following combinations: (1) the wing, body, and high tail fairing; (2) the wing, body, and low tail fairing; (3) the wing, body, and high tail; (4) the wing, body, and low tail; (5) the wing with a 42-percent-span, 15-percent-chord leading-edge extension, body, and low tail.

The majority of the data were obtained at a Reynolds number of 2,000,000 at Mach numbers from 0.20 to 0.92. At a Mach number of 0.20, data were also obtained at a Reynolds number of 11,000,000. Force measurements were made through a range of angles of attack of -10° to 25° for the model with the high tail and -3° to 25° for the model with the low tail, except at the higher Mach numbers where the range was reduced by the limitations of wind-tunnel power and by choking conditions.

The model with the unmodified wing was tested with stabilizer incidences of 0°, $-2\text{-}1/2^{\circ}$, and -5° for both the low and high tail positions. The model with the leading-edge extension and the tail in the low position was tested with the tail at 0° incidence.

Local downwash angles and dynamic-pressure losses in the region of the tail were measured throughout the angle-of-attack ranges for which force and moment data were obtained.

CORRECTIONS TO DATA

The data have been corrected for jet-boundary effects, for constriction due to the tunnel walls, and for model-support tare forces.

Corrections to the data to account for jet-boundary effects due to lift on the wing have been computed by the methods given in reference 8. The corrections, which were added to the angles of attack, drag coefficients, and the pitching-moment coefficients are shown in table II. The data have been corrected for the constriction due to the tunnel walls by the methods of reference 9 and are listed in table II. The

effect of the sweep on the blockage corrections has not been taken into account. Tare corrections to account for the drag due to the exposed area of the turntable were applied by subtracting the values shown in table II from the measured drag coefficients.

No evaluation was made of the interference between the model and the turntable, and no compensation was made for the tunnel-floor boundary layer which had a displacement thickness of 1/2 inch at the turntable.

Corrections to the survey-rake-tube locations were made to account for the displacement of the rake under load. The survey rake was tested separately and rotated in pitch to obtain a calibration of the flow angle tubes for measuring local downwash at the various Mach numbers.

RESULTS AND DISCUSSION

Effect of Tail Height

Lift, drag, and pitching-moment characteristics.- The lift, drag, and pitching-moment characteristics at a Reynolds number of 11,000,000 and a Mach number of 0.20 are shown in figure 3 for the model with the tail in the high position and in figure 4 for the model with the tail in the low position. Data for the tail-off configuration, which are also shown in figures 3 and 4, show an abrupt forward movement of the center of pressure near maximum lift. When the tail was added in the high position there was an even larger forward center-of-pressure movement, indicating that the tail was destabilizing at the higher lift coefficients. Adding the tail in the low position eliminated practically all the forward center-of-pressure movement (fig. 4). Lowering the tail had no effect on the stability characteristics at the lower lift coefficients.

The lift, drag, and pitching-moment characteristics at a Reynolds number of 2,000,000 and at Mach numbers of 0.20 to 0.92 are shown in figure 5 for the model with the tail in the high position and in figure 6 for the model with the tail in the low position. Data for the tail-off configuration, which are also included in figures 5 and 6, indicate the forward movements of center of pressure occurred initially at lower lift coefficients and extended over a greater range of lift coefficients than at a Reynolds number of 11,000,000 and a Mach number of 0.20 (fig. 3). Addition of the tail in the high position resulted in increased stability up to the lift coefficient at which severe instability occurred with the tail off, but above this lift coefficient, the

tail did not increase the stability of the model, and in some instances at the higher lift coefficients the resulting instability was greater than without the tail. Lowering the horizontal tail extended the lift-coefficient range over which the tail increased the stability of the model, reducing the abruptness and the extent of the forward center-of-pressure movement at the high lift coefficients for Mach numbers below 0.90. Lowering the tail failed to improve the longitudinal stability at the high angles of attack at a Mach number of 0.90. At a Mach number of 0.92, addition of the tail in either position resulted in an increase in the static margin throughout the entire lift-coefficient range.

Effective downwash at the tail.- The effective downwash angle at the horizontal tail was computed from the force and moment data and is shown in figures 7 and 8. Figure 7 shows the effect of tail height and Reynolds number on the effective downwash at a Mach number of 0.20 while figure 8 shows the effect of Mach number at a Reynolds number of 2,000,000.

In general, the angles of attack at which large increases in $d\epsilon/d\alpha$ occurred corresponded to the angles of attack at which instability was evidenced in the pitching-moment data (figs. 3 through 6). The data in figures 7 and 8 show that $d\epsilon/d\alpha$ at moderate and high angles of attack increased more rapidly with angle of attack with the tail in the high position than in the low position. It is evident that the varying effects of tail height on tail contribution to stability may be attributed, to a large extent, to the vertical distribution of downwash behind the wing.

Tail stability parameter.- If the rate of change of q_t/q with angle of attack is neglected, the contribution of the horizontal tail to the static longitudinal stability can be represented by the expression:

$$\left(\frac{dC_m}{dC_L}\right)_t = -\left[\frac{(dC_L/d\alpha)_t}{(dC_L/d\alpha)_{w+b}}\left(\eta\frac{q_t}{q}\right)V_t\left(1-\frac{d\epsilon}{d\alpha}\right)\right]$$

This tail stability parameter is shown as a function of the angle of attack in figure 9 for the two tail heights at Mach numbers of 0.60, 0.80, and 0.90. Also shown in figure 9, are the three individual factors which contribute to the total tail effectiveness. The values of $dC_L/d\alpha$ for the horizontal tail alone at the various Mach numbers were obtained from reference 10 and corrected for the small difference in aspect ratio. The tail efficiency factor was computed by means of the equation

$$\eta\left(\frac{q_t}{q}\right) = -\left(\frac{\partial C_m}{\partial i_t}\right) \frac{1}{(dC_L/d\alpha)_t \; V_t}$$

At Mach numbers of 0.80 and below, it is seen that the high tail was ineffective at angles of attack above 10° or 11° because the rate of change of downwash with angle of attack attained a value of unity and, thus, the tail stability parameter went to zero. Lowering the horizontal tail was effective because it placed the tail in a more favorable downwash field for which $d\epsilon/d\alpha$ was always less then unity. Lowering the tail caused a slight reduction in $\eta(q_t/q)$. As will be shown in a following section, this was a result of the low tail moving into the wing wake.

The preceding statements have been restricted to Mach numbers less than 0.80. That the same general effect existed at a Mach number of 0.85 can be seen from inspection of figures 5(d), 6(d), and 8. At a Mach number of 0.90 (fig. 9(c)), the tail contributed to the stability at all angles of attack and there was little effect of varying the vertical height of the horizontal tail. The instability of the complete model at angles of attack above about 7° was a result of the large and abrupt forward shift of the center of pressure of the wing-body combination.

Theoretical downwash at the tail.- The theoretical downwash at the horizontal tail was calculated by the method of reference 11 and is compared with the effective downwash calculated from the measured forces and moments in figure 7. The spanwise distribution of lift on the wing-fuselage combination necessary for the prediction of the downwash was calculated by the method of references 12 and 13 and is shown in figure 10.

In general, the theoretical variation of downwash with angle of attack was in good agreement with the experimental variation in the low angle-of-attack range for both tail heights. The small differences between experimental and theoretical values of $d\epsilon/d\alpha$ (fig. 7) for the high and low tail positions may be attributed to certain assumptions of the theory employed (ref. 11). The assumption that the vortex sheet behind the wing was planar is a probable source of error; the degree to which the sheet was rolled up at the location of the tail is not known. A further source of error probably lies in the failure to take into account the effect of the fuselage, except insofar as it influences the wing lift distribution.

Downwash angles were not accurately predicted at the higher angles of attack. It is known from previous studies that flow separation had

occurred at the wing tip at the higher angles of attack with an accompanying distortion of the span loading that could not be predicted by the theory.

Wing-Wake and Local Downwash Measurements

The dynamic-pressure loss in the wake of the wing-fuselage combination and the angle of local downwash near the horizontal tail are presented in figures 11 through 14.

Location of the wing wake.- The location of the wake has been determined from measurements of the total pressures behind the wing-fuselage combination at a position corresponding to 14 percent of the chord of the tail behind the tail leading edge and at three spanwise stations. The results of these wake measurements are presented as the ratio of the decrement in dynamic pressure at the tail to the free-stream dynamic pressure $\Delta q/q$ as a function of vertical distance from the body center line. Data are presented in figure 11 for angles of attack of 0°, 4°, 8°, 12°, and 16° at a Reynolds number of 11,000,000 and a Mach number of 0.20, and in figure 12 for a Reynolds number of 2,000,000 and at Mach numbers from 0.20 to 0.92. The two vertical locations of the horizontal tail are identified as well as the wing chord plane extended. Of the three survey rakes used, two were located within the tail semispan at positions 0.18 b/2 and 0.33 b/2 from the plane of symmetry, whereas the third was at 0.47 b/2 which was beyond the tip of the tail semispan. Accordingly, the vertical locations of the high and low tail have not been indicated in the figures pertaining to the rake at 0.47 b/2.

At a Reynolds number of 11,000,000 and a Mach number of 0.20, the high tail was completely above the wake at angles of attack up through 16°, whereas the low tail moved into the center of the wake at an angle of attack of 12°. Throughout the Mach number range and at a Reynolds number of 2,000,000 (fig. 12), both the high and low tail are seen to be outside the region of large wake losses at angles of attack of 8° and below. At an angle of attack of 12° (fig. 12(d)), the low tail had moved into the center of the wake, whereas the high tail was still above the wake except at the extreme tip. At 16° angle of attack, the low tail had moved below the center of the wake and the tip of the high tail had moved into the wake at the higher Mach numbers. At the higher angles of attack, the thickness of the wake and its displacement above the chord plane of the wing increased markedly with lateral distance from the plane of symmetry, especially at the higher Mach numbers. This was a direct result of the separation on the outer portion of the wing semispan.

It is obvious from the foregoing that the lower tail passed through the wake in the angle-of-attack range up to 16° whereas the high tail was effectively above the wake except at the extreme tip. The improvements in longitudinal stability at the higher angles of attack as a result of lowering the horizontal tail thus came about in spite of an unfavorable wake effect rather than because of any favorable effect. A still lower tail position would probably benefit from a favorable downwash variation with angle of attack without being penalized by moving into a region of reduced dynamic pressure at the precise angle of attack where the maximum tail contribution to stability is desired.

Local downwash measurements.- Figures 13 and 14 present the variation of local downwash angle with angle of attack for three spanwise stations at a Reynolds number of 11,000,000 and a Mach number of 0.20, and at a Reynolds number of 2,000,000 and Mach numbers from 0.20 to 0.92. It may be noted that only the innermost survey station (0.25 b/2) was within the extremity of the tail span, although the middle downwash station at 0.40 b/2 was just beyond the tip of the tail. The downwash survey was slightly above the low tail postion.

A detailed study of local downwash in the region of the tail was not attempted during tests of the model with the survey rake. The downwash data obtained at the survey-tube locations provided some information in regard to the spanwise distribution of downwash, particularly as this distribution of downwash varied at high angles of attack of the model.

At a Reynolds number of 11,000,000 and a Mach number of 0.20 (fig. 13), $d\epsilon/d\alpha$ was nearly constant up to angle of attack of 12° and showed little variation with spanwise location, except at the outermost survey station at the highest angles of attack. For low angles of attack, the data presented in figure 14 show little variation in the values of $d\epsilon/d\alpha$ with spanwise location throughout the range of test Mach numbers. At the higher angles of attack, the values of $d\epsilon/d\alpha$ increased with increasing spanwise distance at all the Mach numbers. The angles of attack at which the increases in $d\epsilon/d\alpha$ took place corresponded fairly closely with those shown in figure 8 for the effective downwash.

Effect of a Leading-Edge Extension

A previous wind-tunnel investigation of this same model (ref. 4) has shown the effects of various leading-edge chord extensions on the static stability of the model with the high tail. The most effective of these leading-edge chord extensions (0.15 c extension from 0.58 b/2 to tip) has been tested with the tail in the low position, and its effects

on the longitudinal characteristics are presented in figures 15 and 16. At a Reynolds number of 11,000,000 and a Mach number of 0.20 (fig. 15), the lift curve for the model with the leading-edge extension remained linear to a higher angle of attack than for the model with the unmodified wing, resulting in an increase in maximum lift coefficient. At maximum lift the stall was mild without a large loss of lift.

The effect of the leading-edge extension on the lift, drag, and pitching-moment characteristics of the model at various Mach numbers is shown in figure 16. The pitching-moment data (fig. 16(b)) indicate that addition of the leading-edge chord extension eliminated or delayed to higher lift coefficients the forward shift of the center of pressure at Mach numbers below 0.90. The lift and drag data in figure 16 indicate an increase of lift-curve slope and a decrease of drag coefficient at the higher lift coefficients for the same range of Mach numbers. A comparison of the pitching-moment data for this model at these Mach numbers with data presented in reference 4 for the model with the high tail indicates a greater static margin at all the higher lift coefficients when the tail was in the low position. However, the effect of the leading-edge extension on the stability in the high-lift-coefficient range was slightly smaller with the tail in the low position (fig. 16(b)) than in the high position (ref. 4). Similar observations were made from another investigation of leading-edge extensions with variable tail height (ref. 5). At a Mach number of 0.90, the lift coefficient at which a forward shift of the aerodynamic center occurred was decreased slightly by lowering the tail although the total center-of-pressure movement was not as large as with the high tail. At a Mach number of 0.92, the pitching-moment characteristics remained essentially unaltered with addition of the leading-edge extension.

CONCLUSIONS

An investigation has been made of the effects of horizontal-tail height and of a 42-percent-semispan, leading-edge chord extension on the longitudinal characteristics of a model with a 35° sweptback wing. The results of these tests and of air-stream surveys in the region of the horizontal tail indicate the following:

1. Lowering the tail from 22 percent to 8 percent of the wing semispan above the wing chord plane extended reduced the forward movement of the center of pressure of the model with the unmodified wing at moderate to high lift coefficients at all Mach numbers up to 0.90 and at a Reynolds number of 2,000,000. At a Reynolds number of 11,000,000 and a Mach number of 0.20, lowering the tail practically eliminated the forward center-of-pressure movement. The variation of calculated downwash angles with angle of attack indicated that there were adverse stability

effects due to a region of large downwash at the position of the high tail and that they could be partially avoided by locating the tail in the low position. However, at Mach numbers of 0.90 and above, no large adverse effects of downwash were observed and the variations of stability with lift coefficient could be attributed largely to the longitudinal characteristics of the wing and fuselage. Lowering the tail at these Mach numbers had little effect on the stability.

2. Wake surveys in the region of the tail indicated that the efficiency of the low tail was reduced somewhat by the fact that it moved into the center of the wing wake at moderate angles of attack.

3. Addition of the wing leading-edge extension to the model with the low tail eliminated the forward movement of the aerodynamic center at moderate lift coefficients for Mach numbers up to 0.90, but provided little change at Mach numbers of 0.90 and 0.92.

Ames Aeronautical Laboratory
National Advisory Committee for Aeronautics
Moffett Field, Calif., Oct. 7, 1953

REFERENCES

1. Anderson, Seth B., and Bray, Richard S.: A Flight Evaluation of the Longitudinal Stability Characteristics Associated With the Pitch-Up of a Swept-Wing Airplane in Maneuvering Flight at Transonic Speeds. NACA RM A51I12, 1951.

2. McFadden, Norman M., Rathert, George A., Jr., and Bray, Richard S.: The Effectiveness of Wing Vortex Generators in Improving the Maneuvering Characteristics of a Swept-Wing Airplane at Transonic Speeds. NACA RM A51J18, 1952.

3. Bray, Richard S.: The Effects of Fences on the High-Speed Longitudinal Stability of a Swept-Wing Airplane. NACA RM A53F23, 1953.

4. Selan, Ralph, and Bandettini, Angelo: The Effects of Leading-Edge Extensions, a Trailing-Edge Extension, and a Fence on the Static Longitudinal Stability of a Wing-Fuselage-Tail Combination Having a Wing With 35° of Sweepback and an Aspect Ratio of 4.5. NACA RM A53E12, 1953.

5. Morrison, William D., Jr., and Alford, William J., Jr.: Effects of Horizontal-Tail Height and a Wing Leading-Edge Modification Consisting of a Full-Span Flap and a Partial-Span Chord-Extension on the Aerodynamic Characteristics in Pitch at High Subsonic Speeds of a Model with a 45° Sweptback Wing. NACA RM L53E06, 1953.

6. Spooner, Stanley H., and Martina, Albert P.: Longitudinal Stability Characteristics of a 42° Sweptback Wing and Tail Combination at a Reynolds Number of 6.8×10^{6}. NACA RM L8E12, 1948.

7. Queijo, M. J., and Wolhart, Walter D.: Wind-Tunnel Investigation of the Effects of Horizontal-Tail Position on the Low-Speed Longitudinal Stability Characteristics of an Airplane Model with a 35° Sweptback Wing Equipped with Chordwise Fences. NACA RM L51H17.

8. Sivells, James C., and Salmi, Rachel M.: Jet-Boundary Corrections for Complete and Semispan Swept Wings in Closed Circular Wind Tunnels. NACA TN 2454, 1951.

9. Herriot, John G.: Blockage Corrections for Three-Dimensional-Flow Closed-Throat Wind Tunnels, With Consideration of the Effect of Compressibility. NACA Rep. 995, 1950. (Formerly NACA RM A7B28)

10. Nelson, Warren H., and McDevitt, John B.: The Transonic Characteristics of 17 Rectangular, Symmetrical Wing Models of Varying Aspect Ratio and Thickness. NACA RM A51A12, 1951.

11. Diederich, Franklin W.: Charts and Tables for Use in Calculations of Downwash of Wings of Arbitrary Plan Form. NACA TN 2353, 1951.

12. Schneider, William C.: A Comparison of the Spanwise Loading Calculated by Various Methods with Experimental Loading Obtained on a 45° Sweptback Wing of Aspect Ratio 8 at a Reynolds Number of 4.0×10^{6}. NACA RM L51G30, 1952.

13. Martina, Albert P.: The Interference Effects of a Body on the Spanwise Load Distributions of Two 45° Sweptback Wings of Aspect Ratio 8 from Low-Speed Tests at a Reynolds Number of 4×10^{6}. NACA RM L51K23, 1952.

TABLE I.- GEOMETRY OF THE MODEL

Wing (without leading-edge extension)	
Aspect ratio	4.5
Taper ratio	0.5
Sweep of quarter-chord line	35°
Section normal to quarter-chord line	64A010
Area (semispan) sq ft	4.443
Mean aerodynamic chord, ft	1.458
Dihedral, deg	0
Incidence, deg	0.5
Position on body	mid-wing
Wing (leading-edge extension)	
Extension of chord ahead of normal leading edge	0.15c
Position of inboard extremity of leading-edge extension	0.58 b/2
Body	
Fineness ratio	12.5
Length, ft	7.292
Frontal area/wing area	0.0303
Horizontal Tail	
Aspect ratio	4.333
Taper ratio	1.0
Sweep, deg	0
Section	NACA 63A004
Area (semispan), sq ft	0.542
Tail length (l_t)	2.24 $\bar{c}$
Vertical distance above wing chord plane extended	
High tail	0.22 b/2
Low tail	0.08 b/2
Incidence of tail	0°, $-2\text{-}1/2^{\circ}$, and -5°
Tail volume, $S_t l_t / S_w \bar{c}$	0.273
Survey rake	
Total-pressure-tube locations	
Longitudinal distance from quarter-chord point of wing to total-pressure tubes	2.20 $\bar{c}$

TABLE I.- GEOMETRY OF THE MODEL - Concluded

Extent of vertical distance covered by total-pressure tubes in reference to wing chord plane extended	
Below wing chord plane extended	0.04 b/2
Above wing chord plane extended	0.28 b/2
Spanwise positions of total-pressure tubes .	0.18 b/2 (0.53 $b_t/2$)
	0.33 b/2 (0.95 $b_t/2$)
	0.47 b/2 (1.38 $b_t/2$)
Downwash-tube locations	
Longitudinal distance from quarter-chord point of wing to survey tube	1.92 $\bar{c}$
Vertical distance of survey tubes above extended chord plane	0.12 b/2
Spanwise stations of survey tubes	0.25 b/2 (0.74 $b_t/2$)
	0.40 b/2 (1.16 $b_t/2$)
	0.54 b/2 (1.59 $b_t/2$)

TABLE II.- CORRECTIONS TO DATA

(a) Corrections for Jet-Boundary Effects

M	$\Delta\alpha/C_L$	$\Delta C_D/C_L^2$	$\Delta C_m/C_L$	
			Wing-body	Wing-body-tail
0.20	0.384	0.00590	0.0010	0.0044
.60	.397	.00600	.0016	.0061
.80	.415	.00607	.0020	.0077
.85	.424	.00605	.0023	.0084
.90	.438	.00602	.0027	.0097
.92	.445	.00601	.0031	.0104

(b) Corrections for constriction due to tunnel walls

Corrected Mach number	Uncorrected Mach number	$\frac{q \text{ corrected}}{q \text{ uncorrected}}$
0.200	0.200	1.002
.600	.599	1.003
.800	.797	1.005
.850	.846	1.006
.900	.892	1.010
.920	.909	1.012

(c) Tare corrections

$R \times 10^{-6}$	M	$C_{D_{tare}}$
11	0.20	0.0043
2	.20	.0045
2	.60	.0045
2	.80	.0050
2	.85	.0053
2	.90	.0057
2	.92	.0060

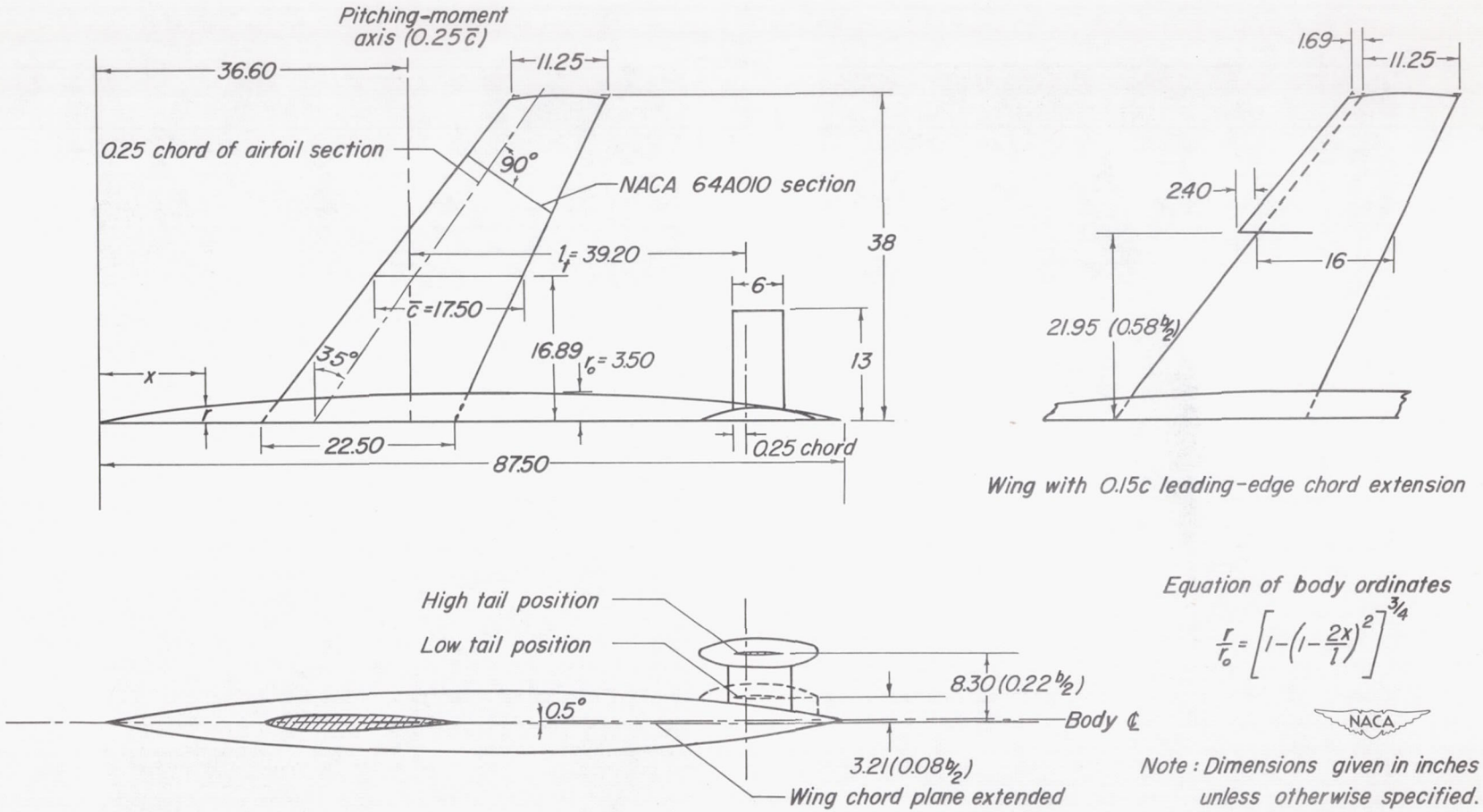

Figure 1.- Drawing of the complete model.

(a) Model with tail in high position.

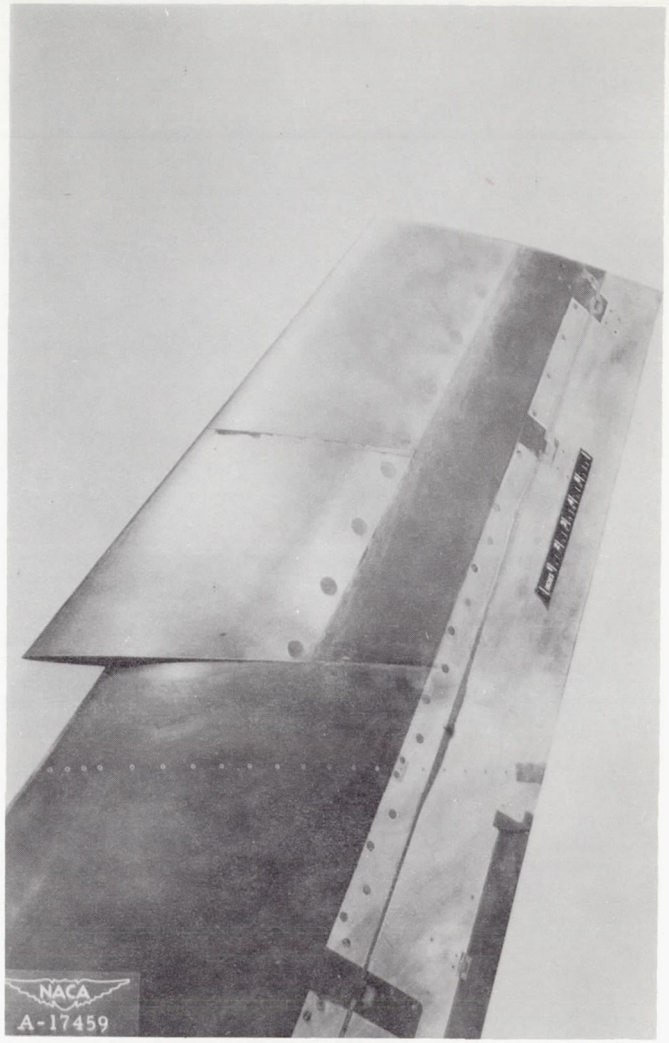

(b) Leading-edge extension.

Figure 2.- Photographs of the model.

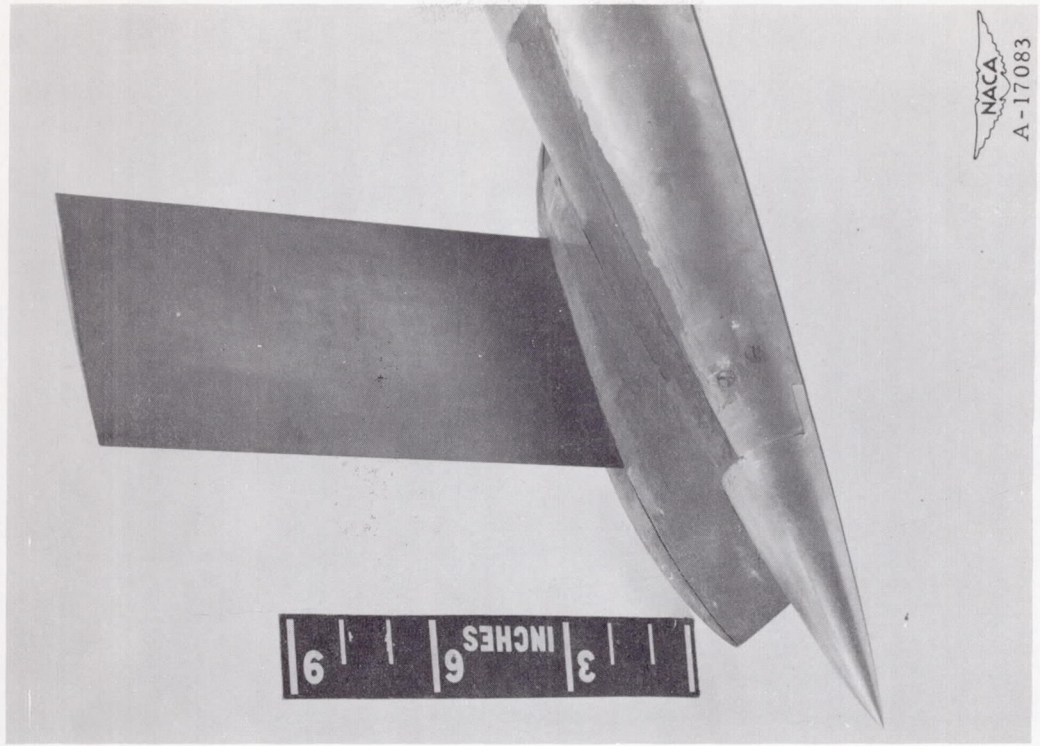

(d) Low tail position.

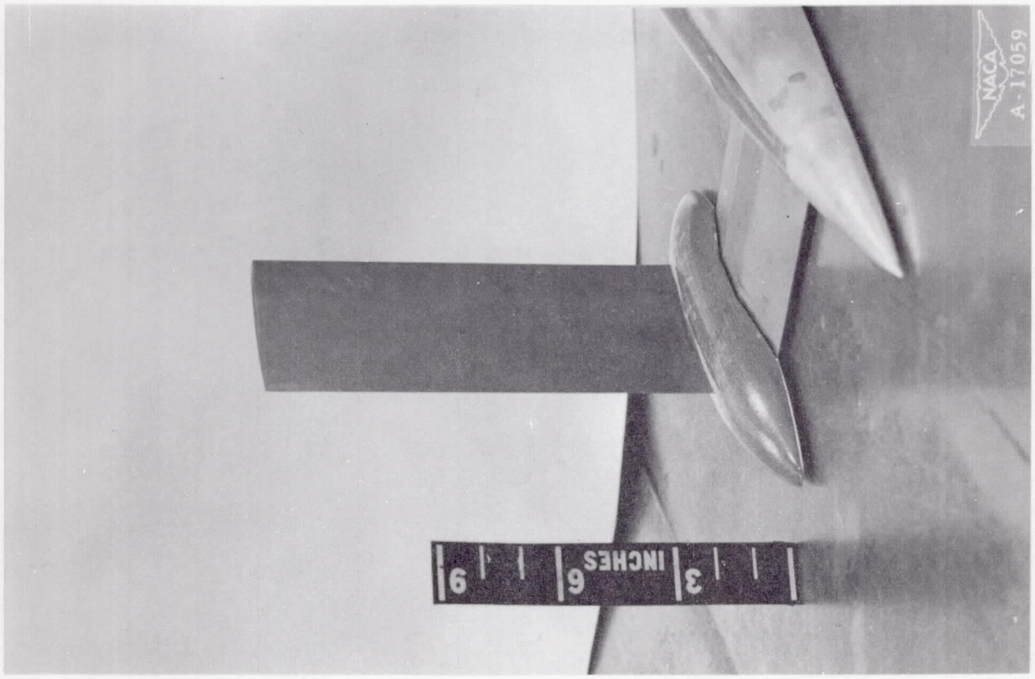

(c) High tail position.

Figure 2.- Continued.

(e) Model with rake attached.

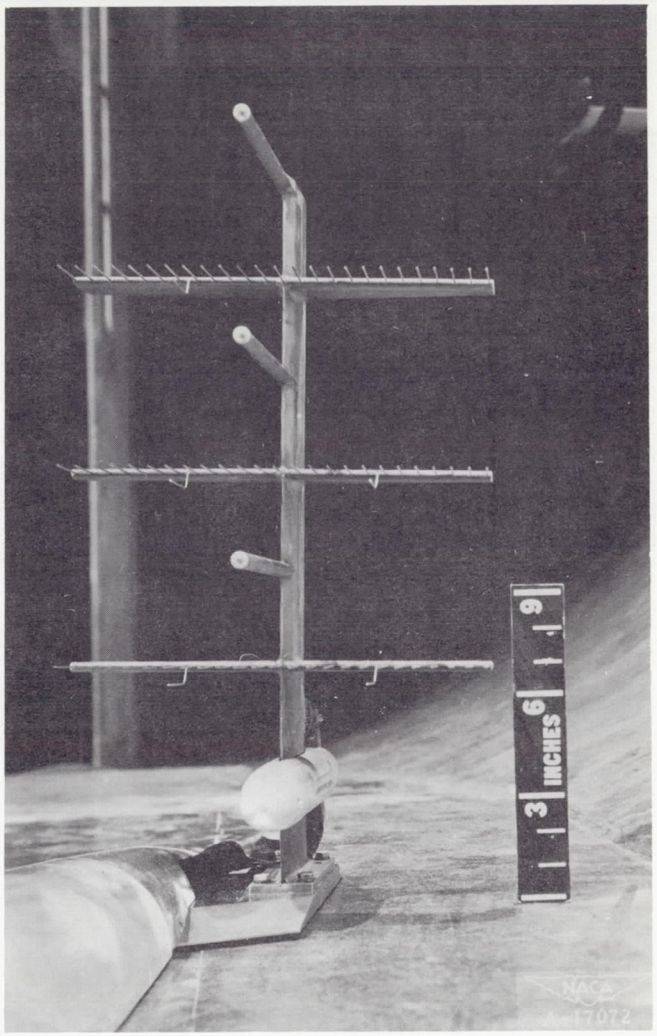

(f) Wake survey rake.

Figure 2.- Concluded.

CONFIDENTIAL

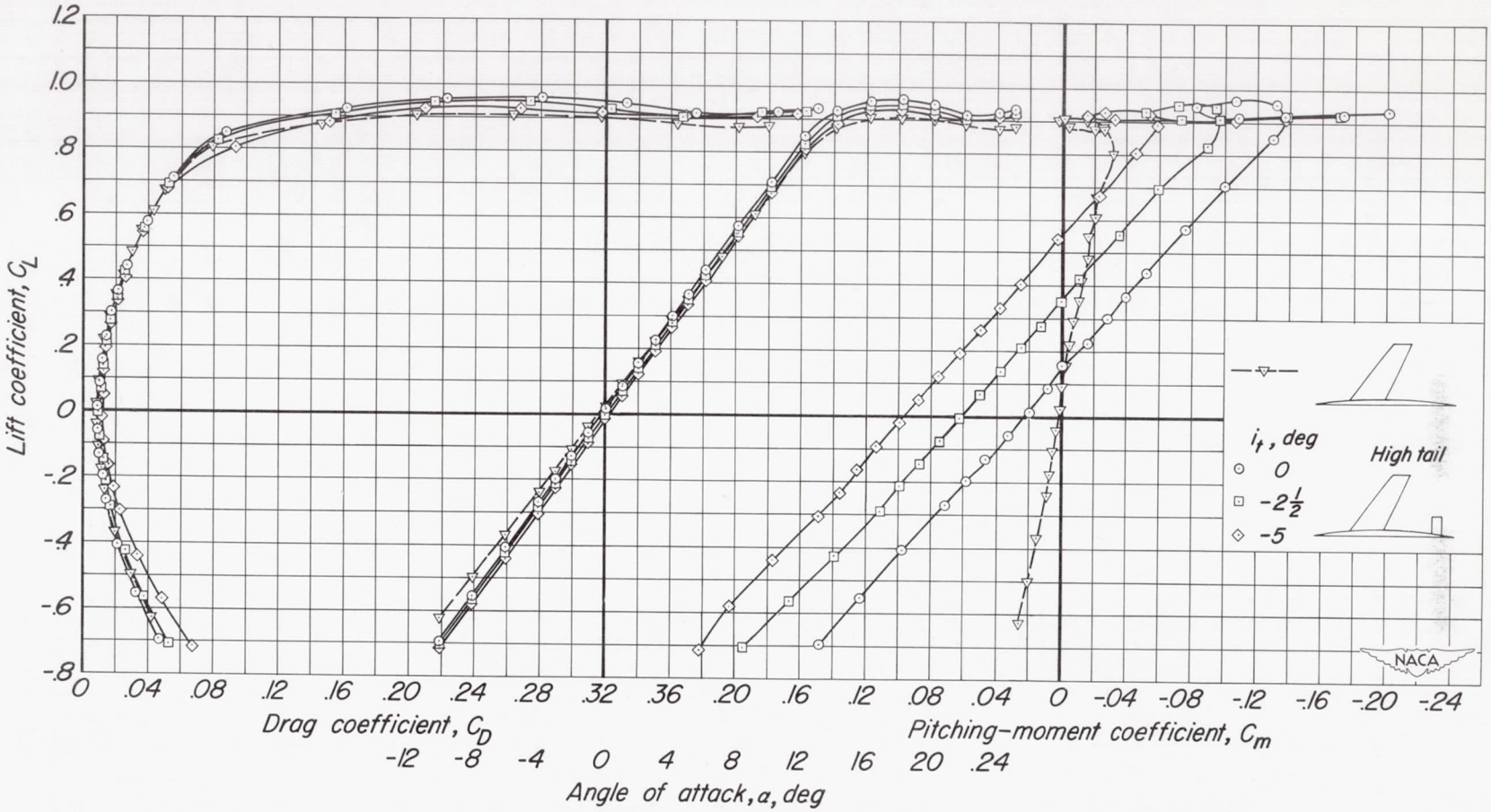

Figure 3.- The lift, drag, and pitching-moment characteristics of the model with the tail in the high position at a Reynolds number of 11,000,000; M = 0.20.

CONFIDENTIAL

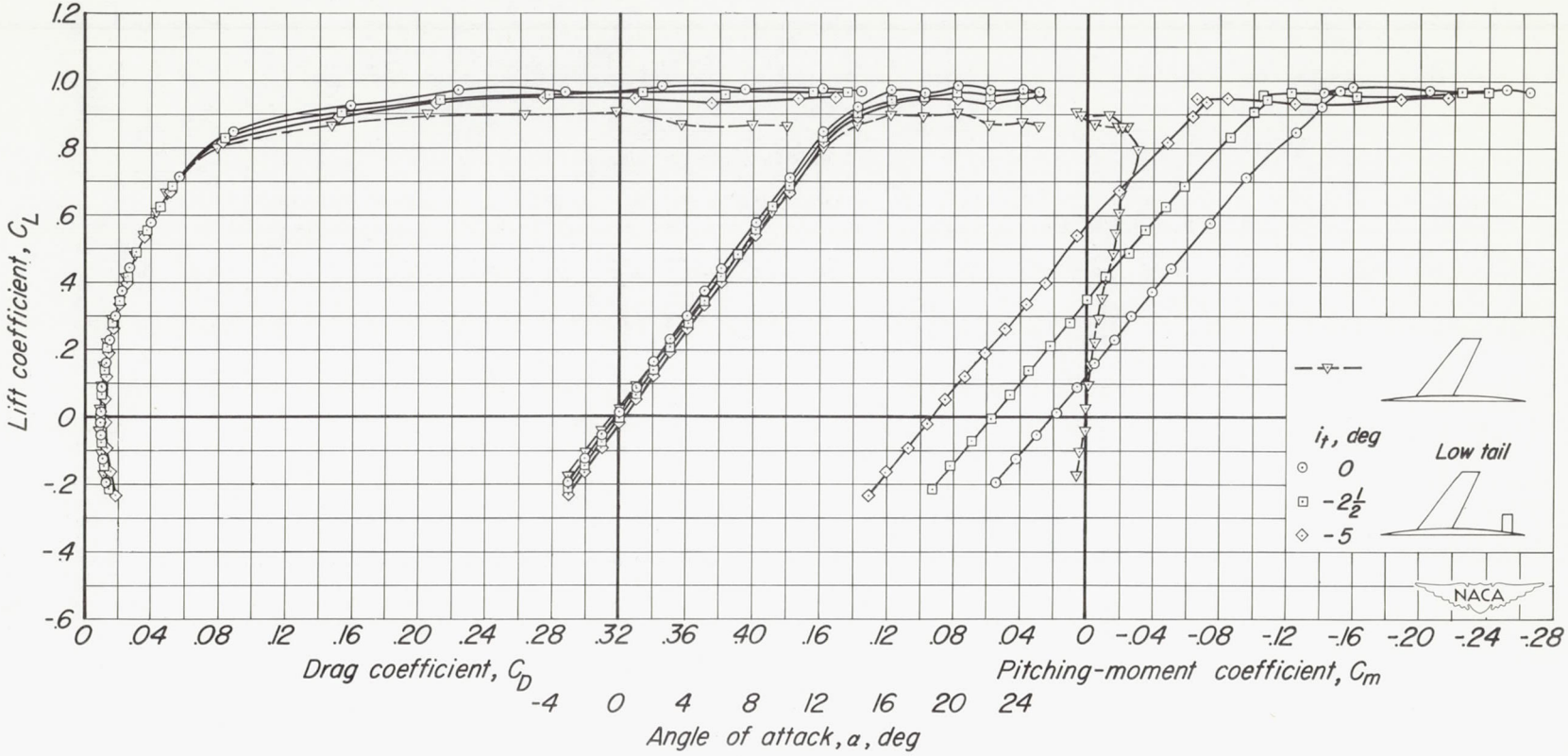

Figure 4.- The lift, drag, and pitching-moment characteristics of the model with the tail in the low position at a Reynolds number of 11,000,000; M = 0.20.

CONFIDENTIAL

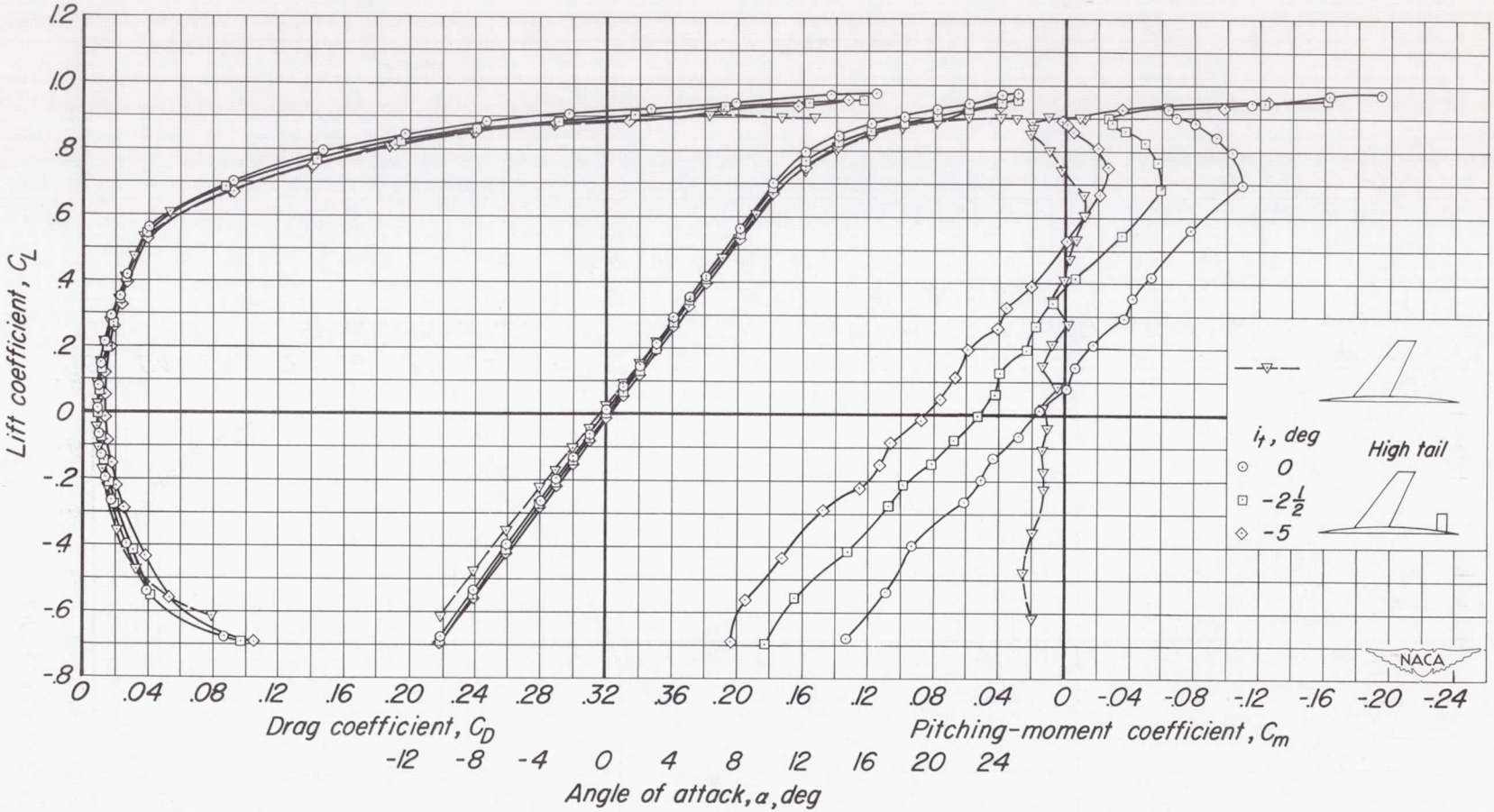

(a) M = 0.20

Figure 5.- The lift, drag, and pitching-moment characteristics of the model with the tail in the high position at a Reynolds number of 2,000,000.

CONFIDENTIAL

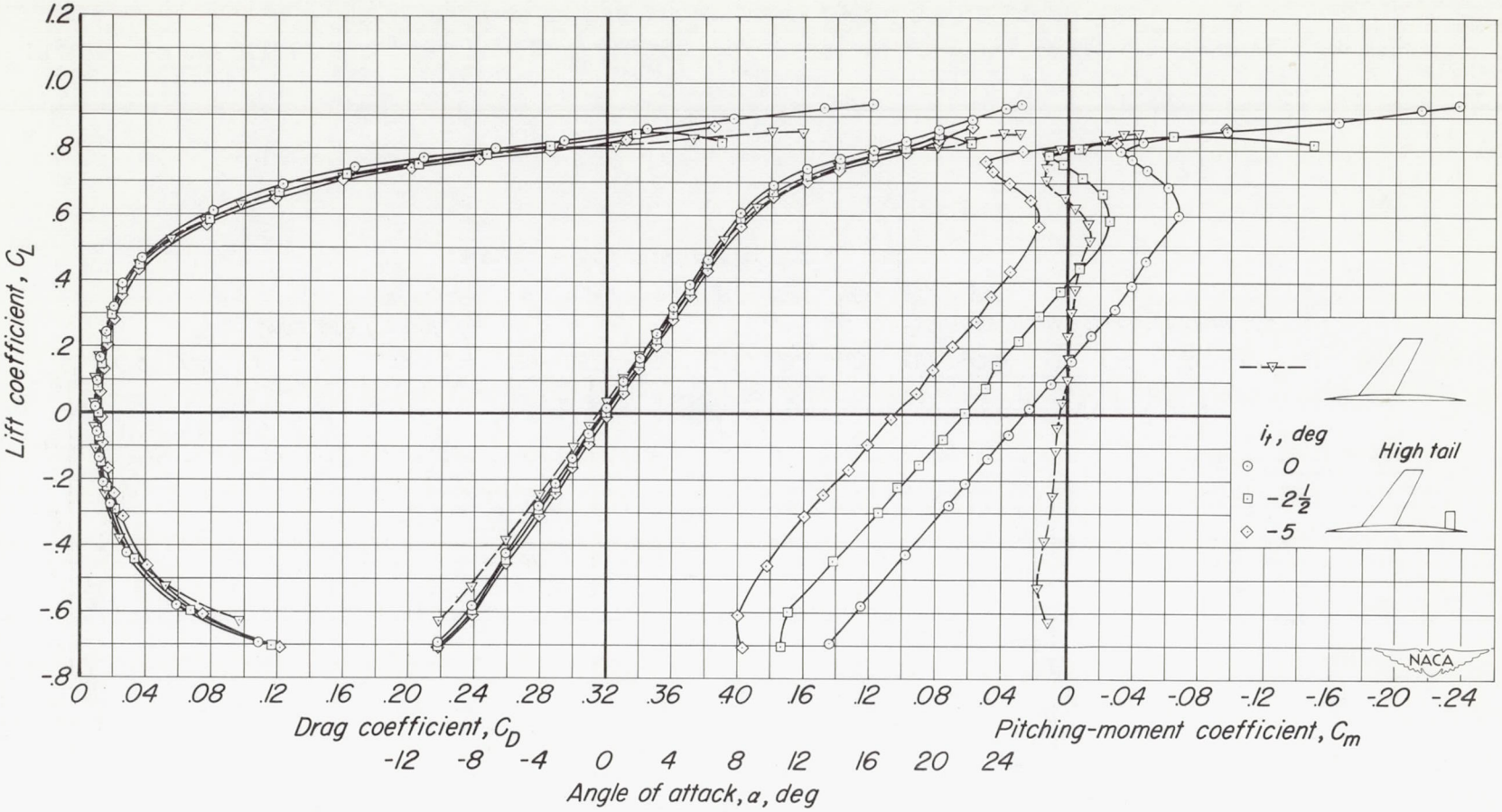

(b) M = 0.60

Figure 5.- Continued.

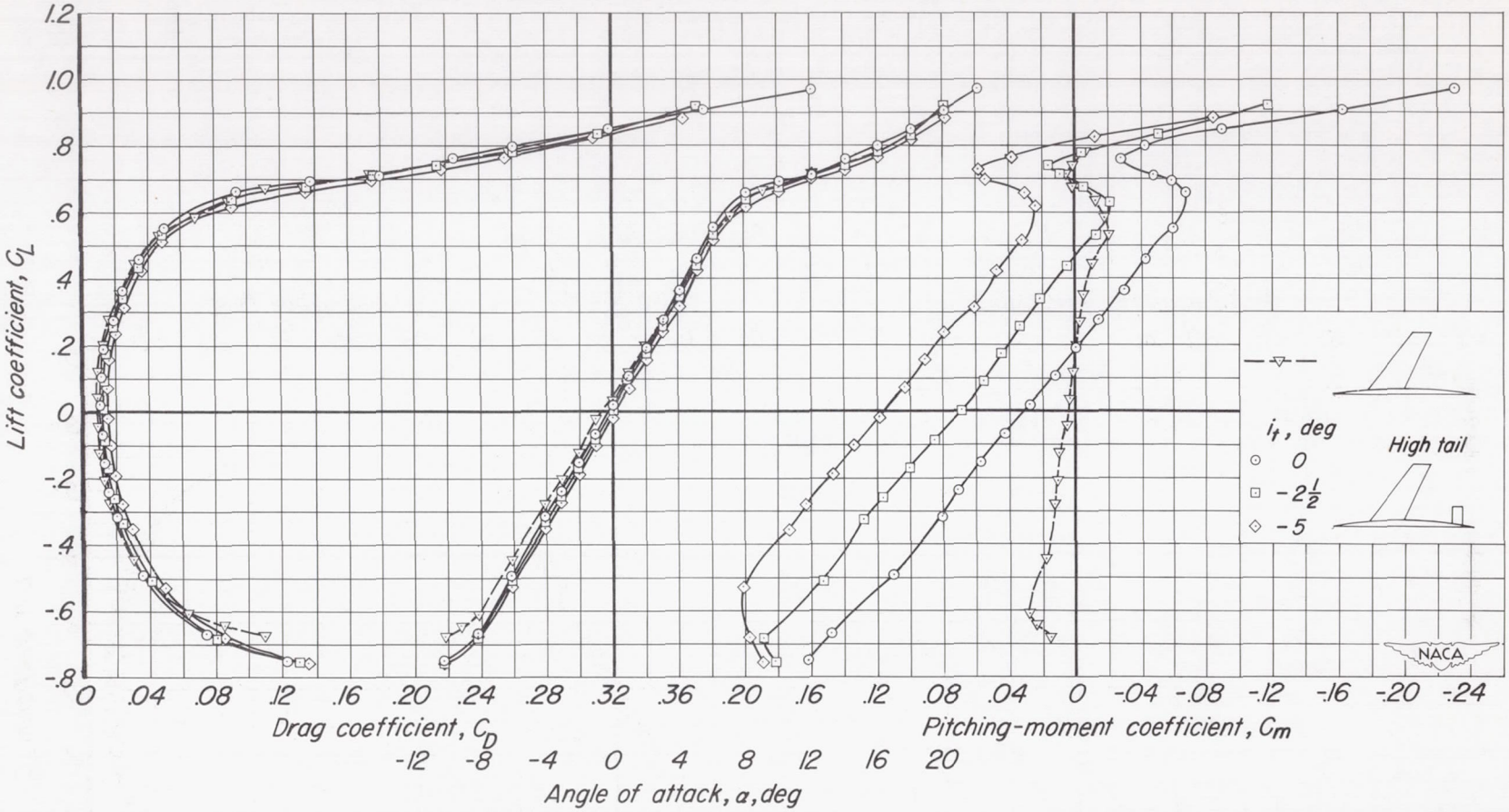

(c) M = 0.80

Figure 5.- Continued.

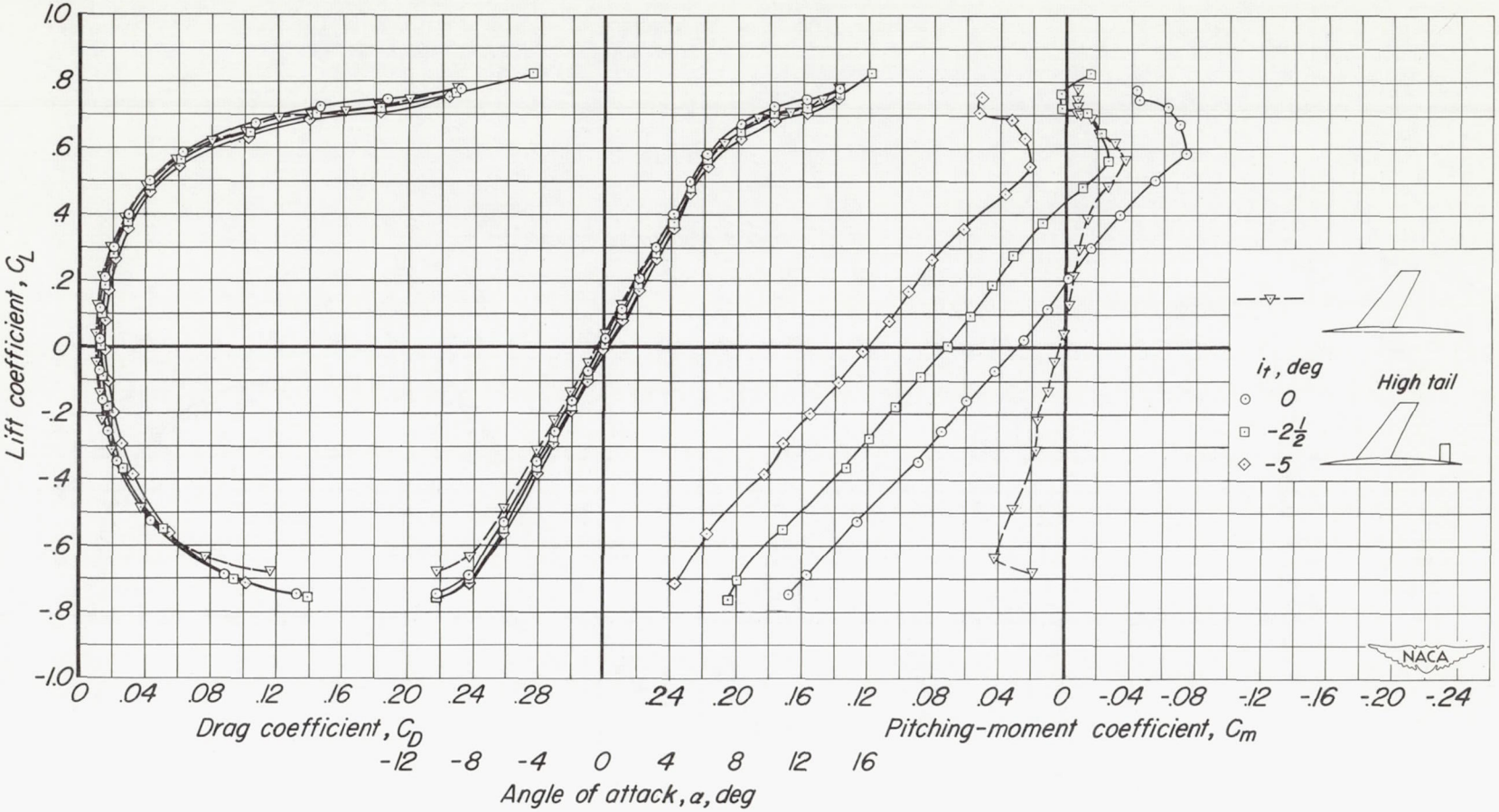

(d) M = 0.85

Figure 5.- Continued.

CONFIDENTIAL

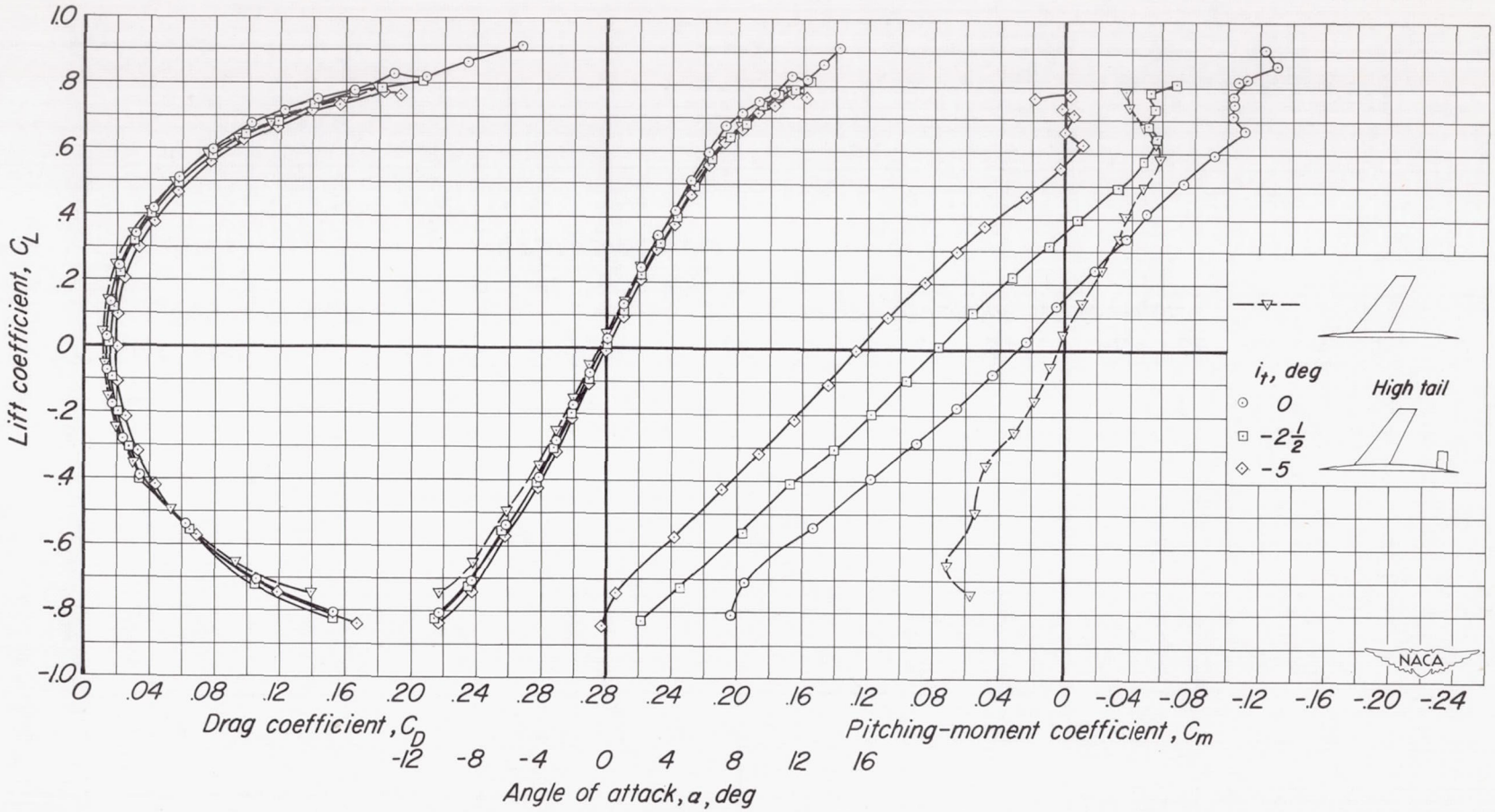

(e) M = 0.90

Figure 5.- Continued.

CONFIDENTIAL

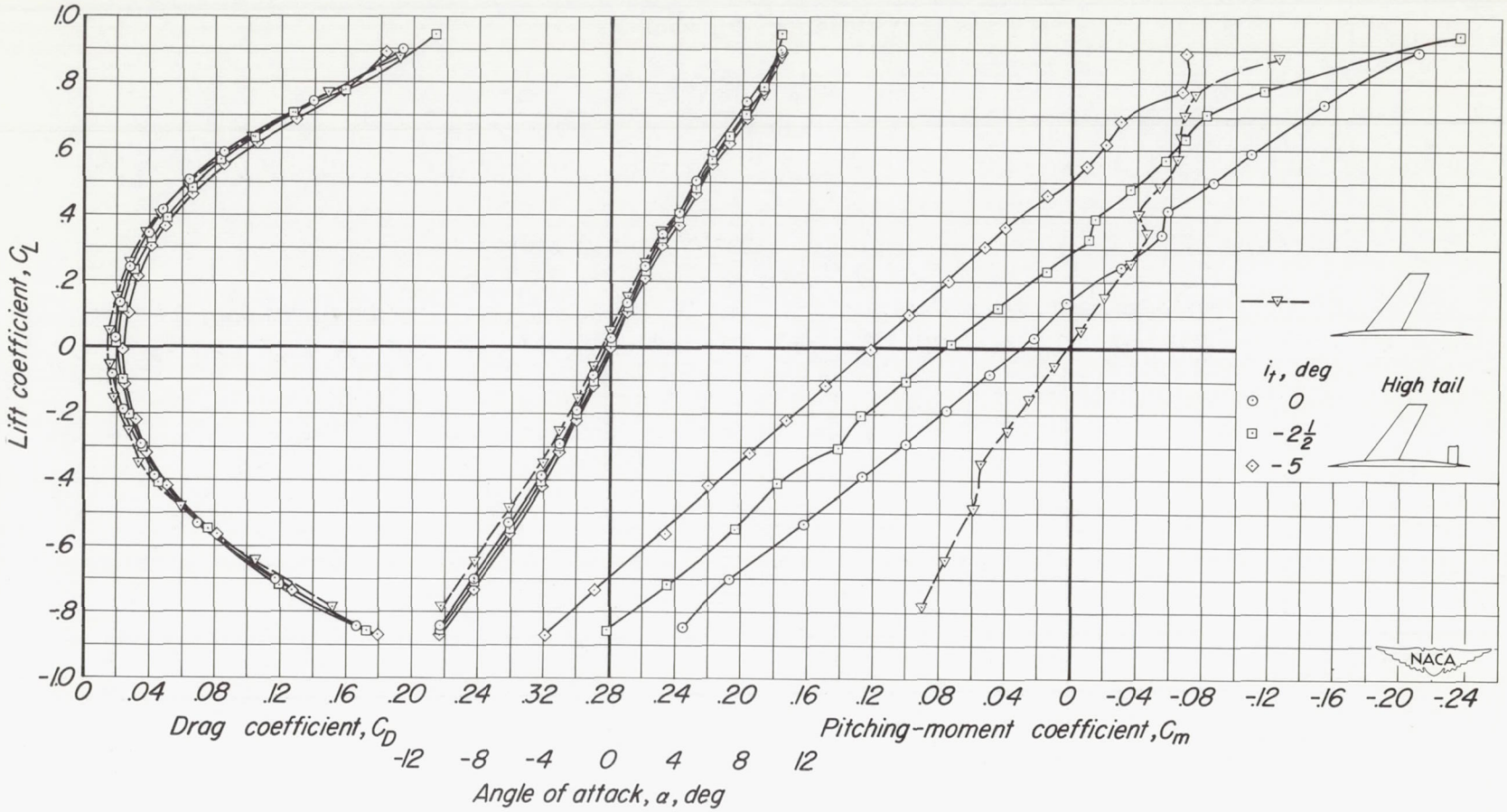

(f) M = 0.92

Figure 5.- Concluded.

CONFIDENTIAL

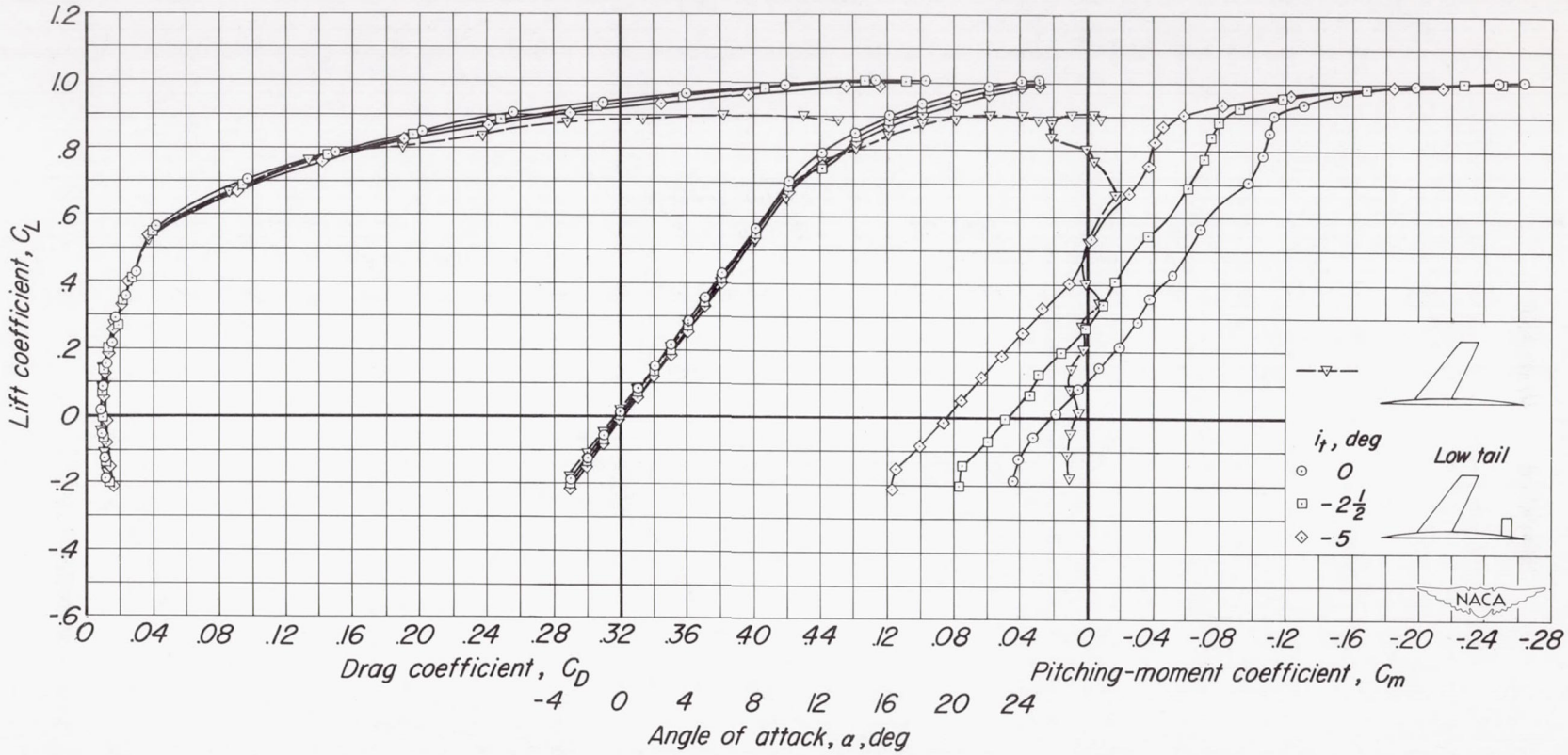

(a) M = 0.20

Figure 6.- The lift, drag, and pitching-moment characteristics of the model with the tail in the low position at a Reynolds number of 2,000,000.

CONFIDENTIAL

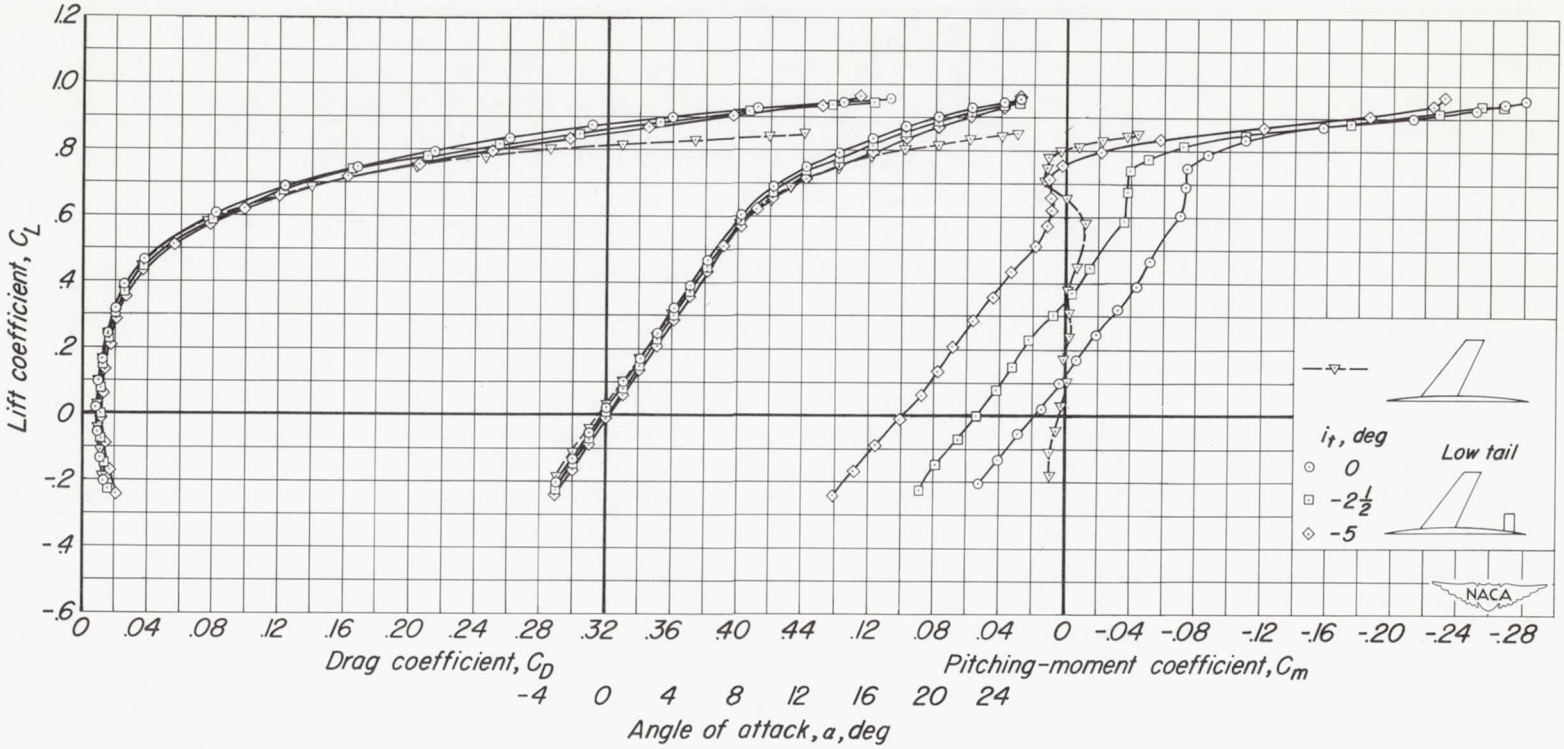

(b) M = 0.60

Figure 6.- Continued.

CONFIDENTIAL

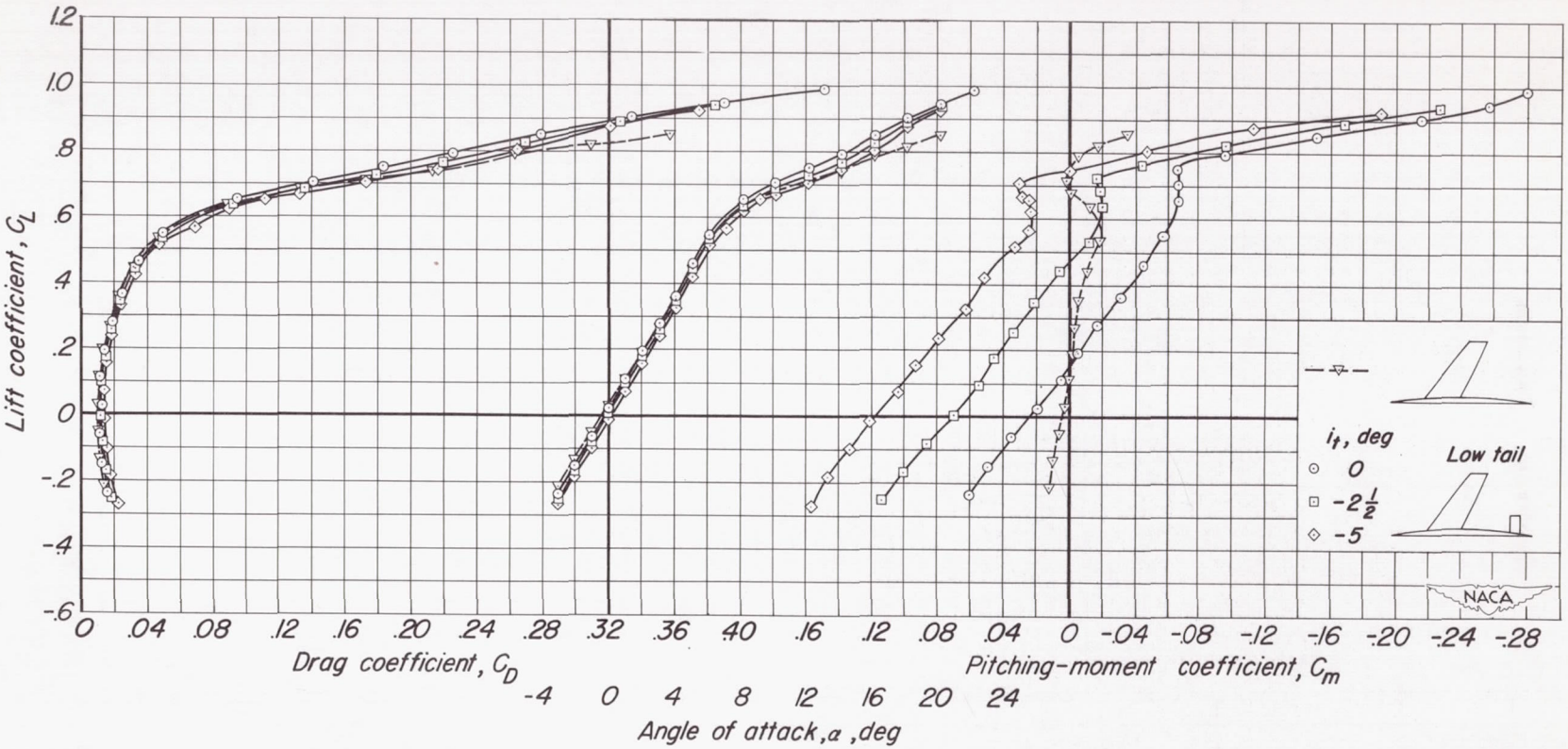

(c) M = 0.80

Figure 6.- Continued.

CONFIDENTIAL

CONFIDENTIAL

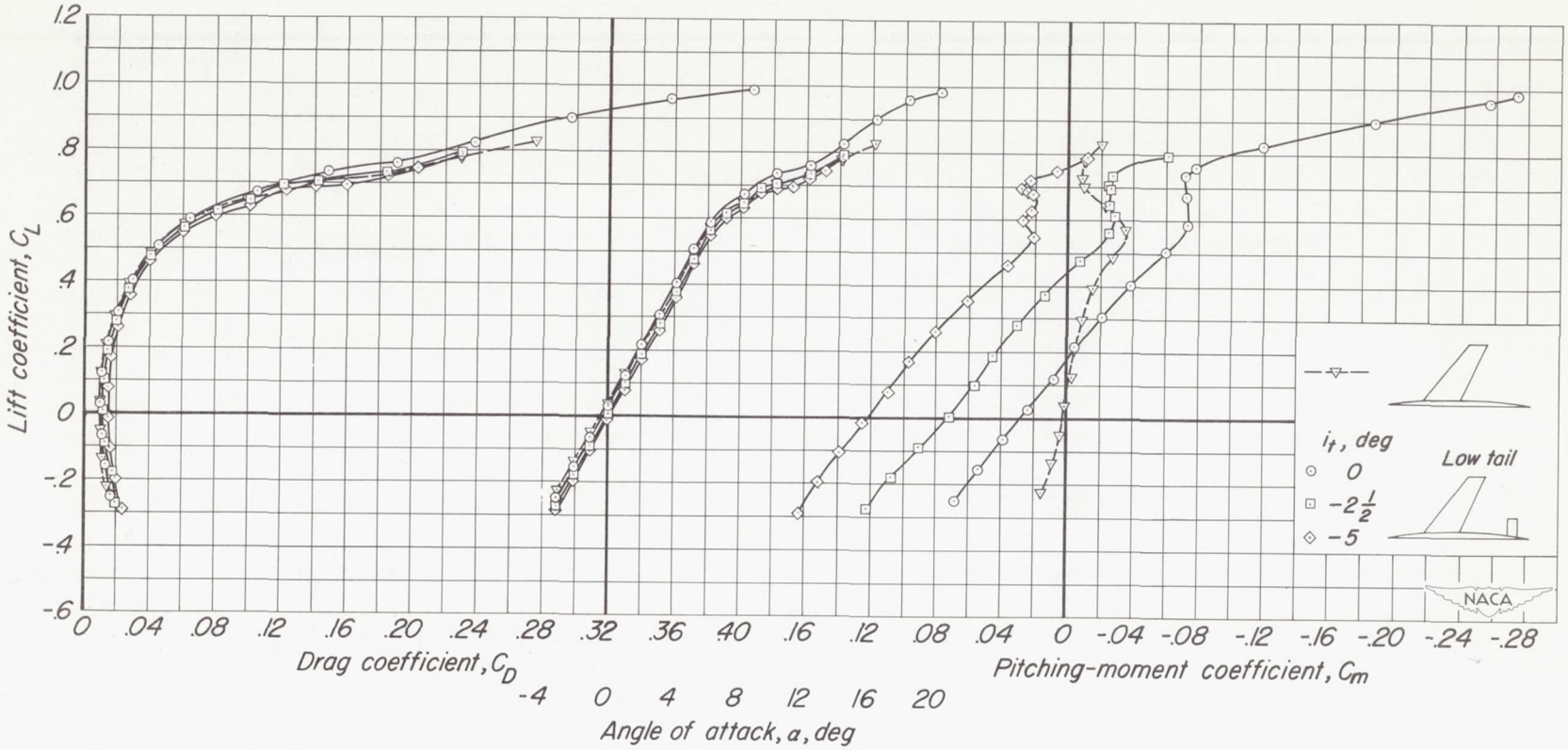

(d) M = 0.85

Figure 6.- Continued.

CONFIDENTIAL

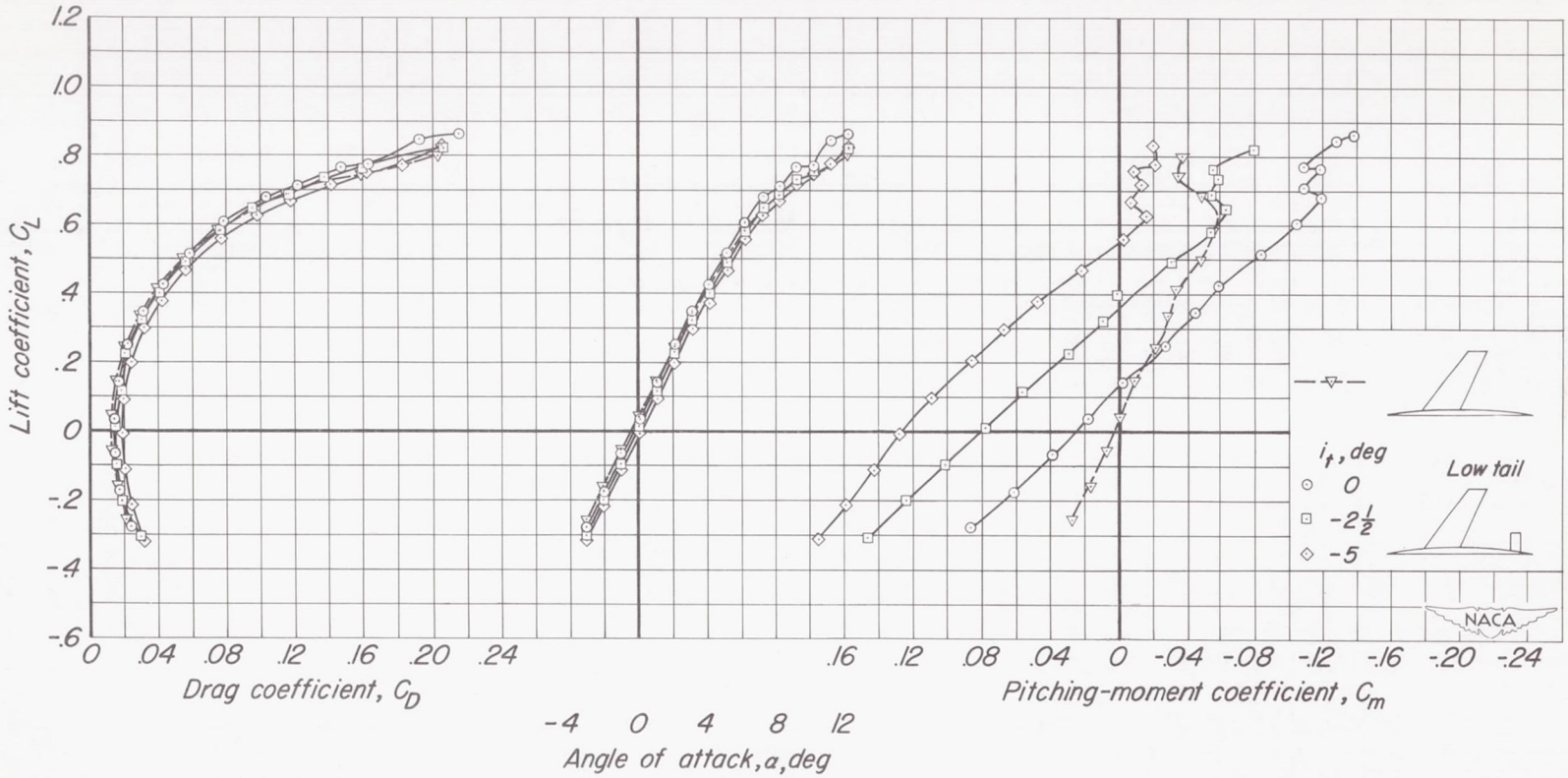

(e) M = 0.90

Figure 6.- Continued.

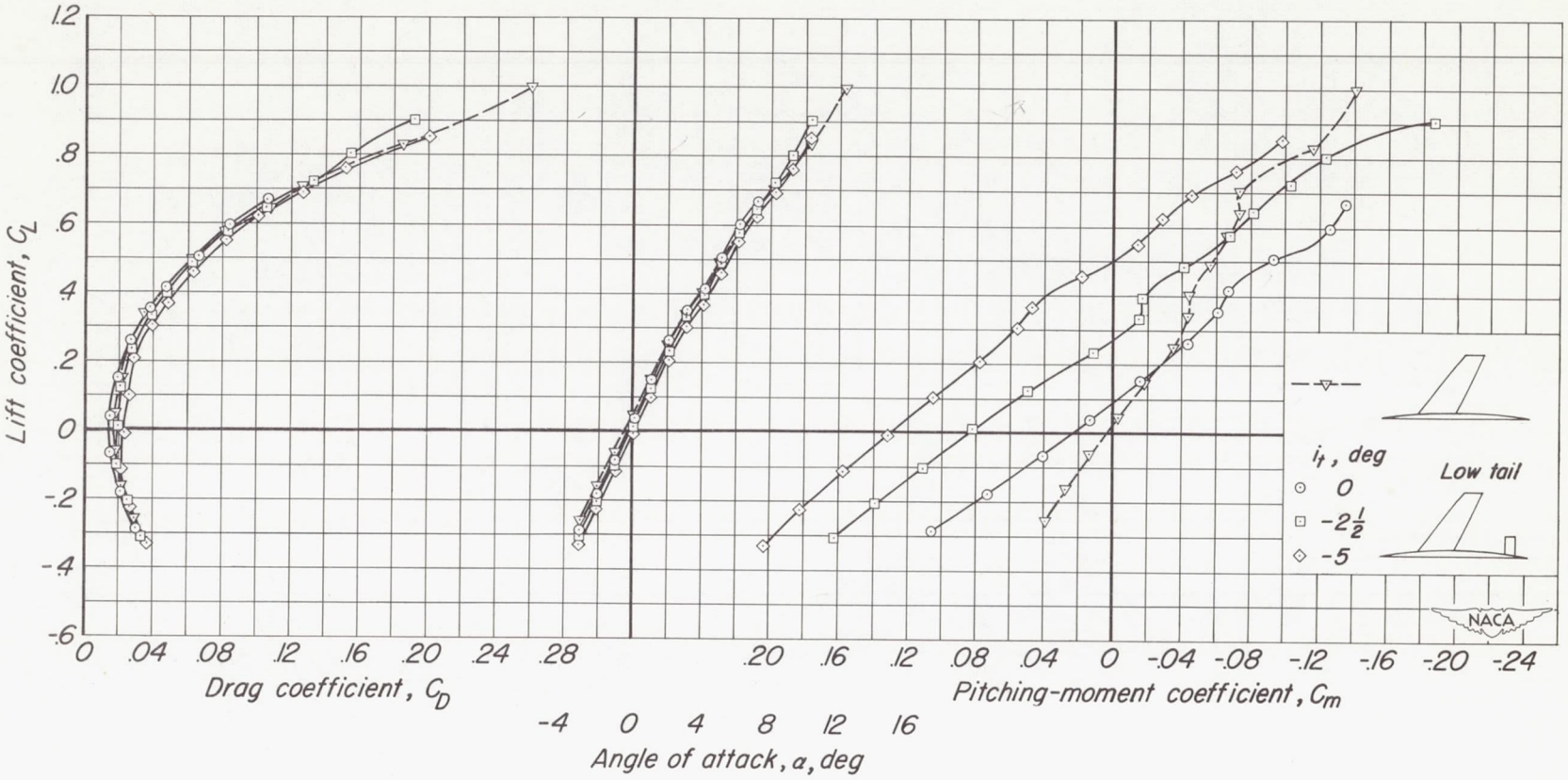

(f) M = 0.92

Figure 6.- Concluded.

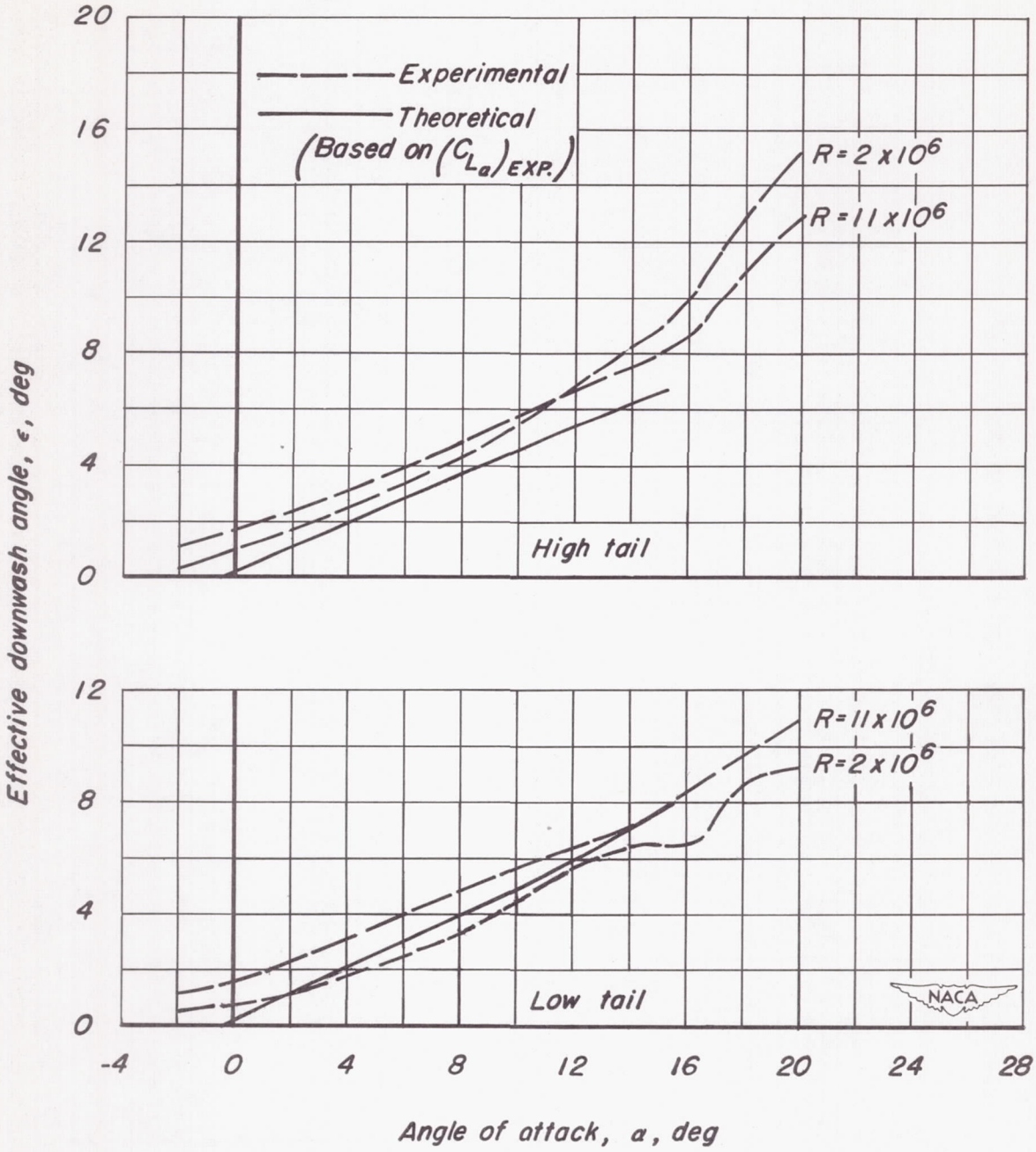

Figure 7.- Comparison of effective wing downwash at the tail with the theoretical downwash; M = 0.20.

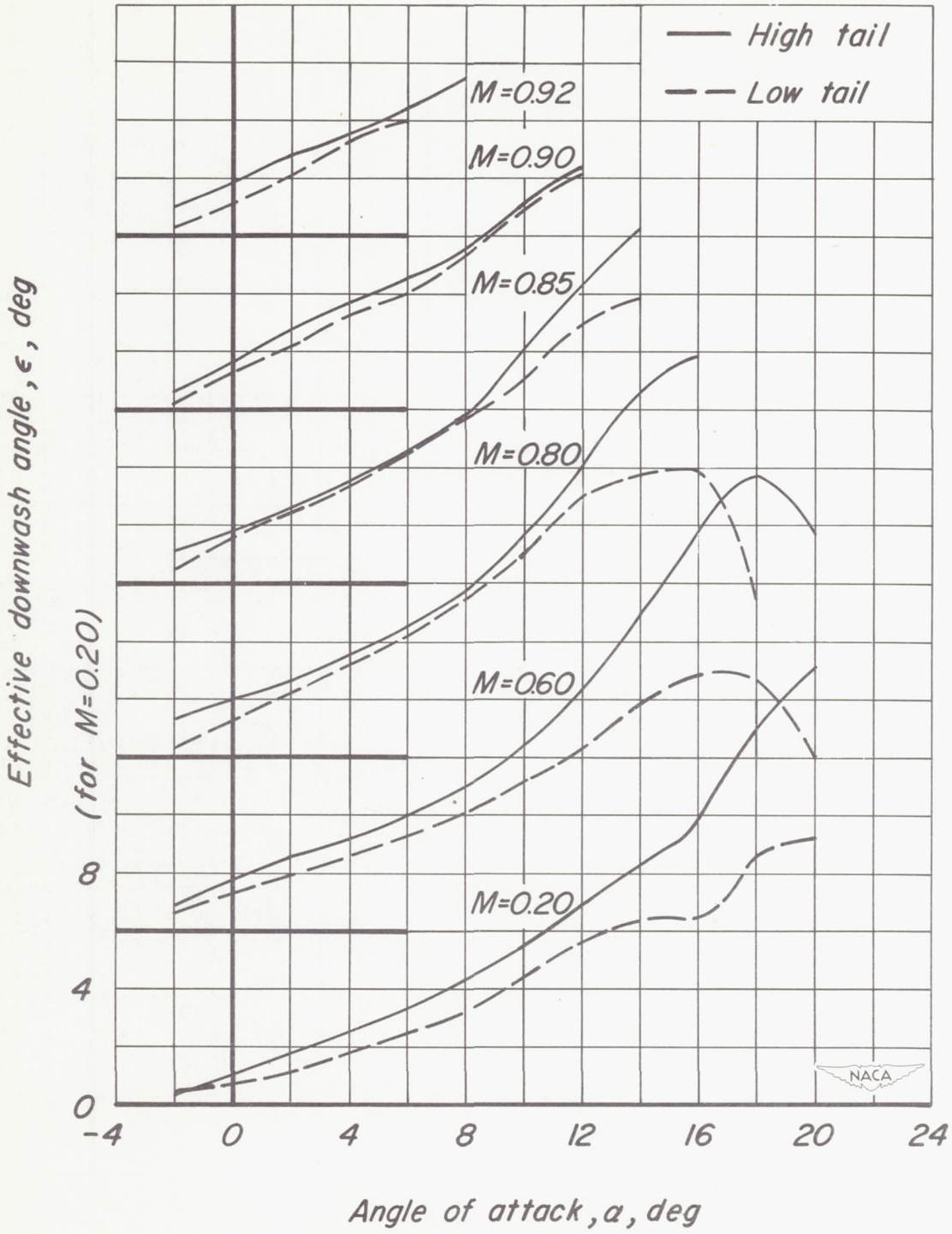

Figure 8.- The variation of effective downwash angle at the tail with angle of attack for various Mach numbers; R = 2,000,000.

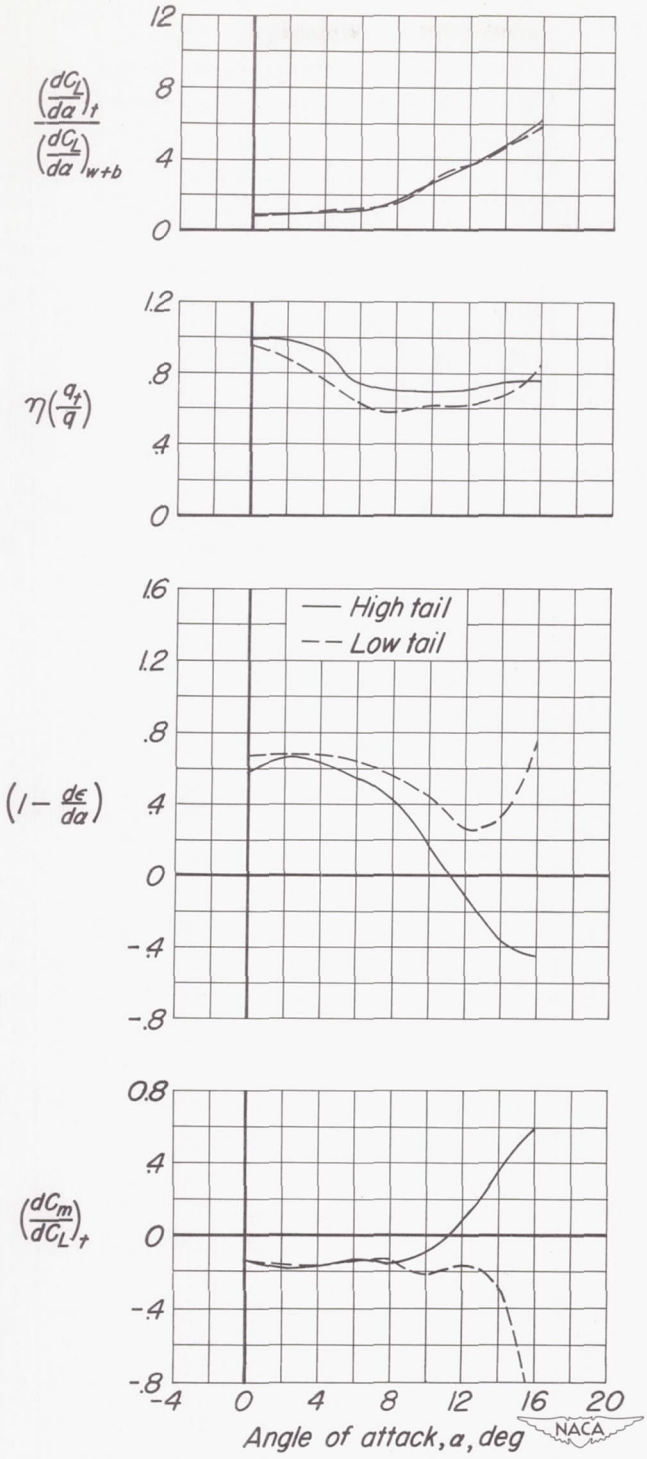

(a) M = 0.60

Figure 9.- The variation with angle of attack of the tail stability parameter and the factors affecting the stability contribution of the horizontal tail; R = 2,000,000.

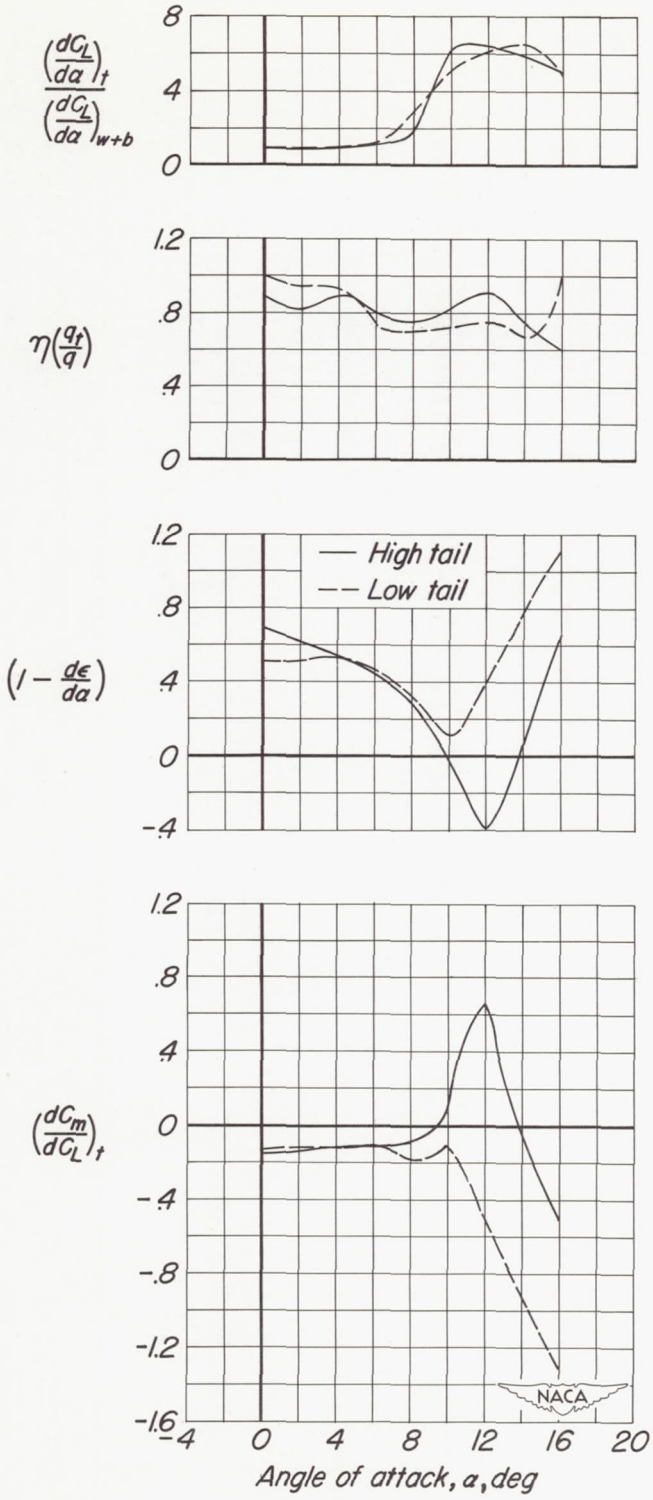

(b) M = 0.80

Figure 9.- Continued.

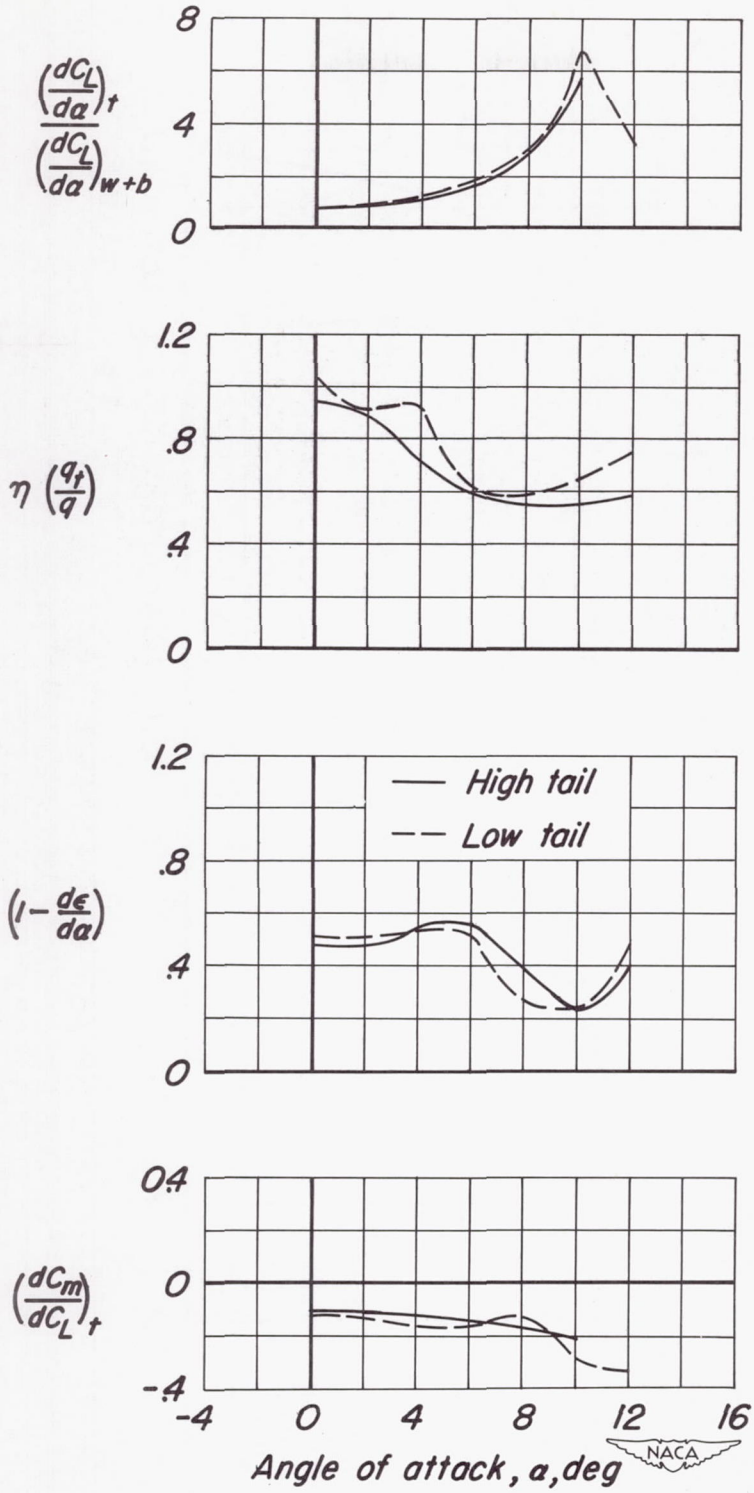

(c) M = 0.90

Figure 9.- Concluded.

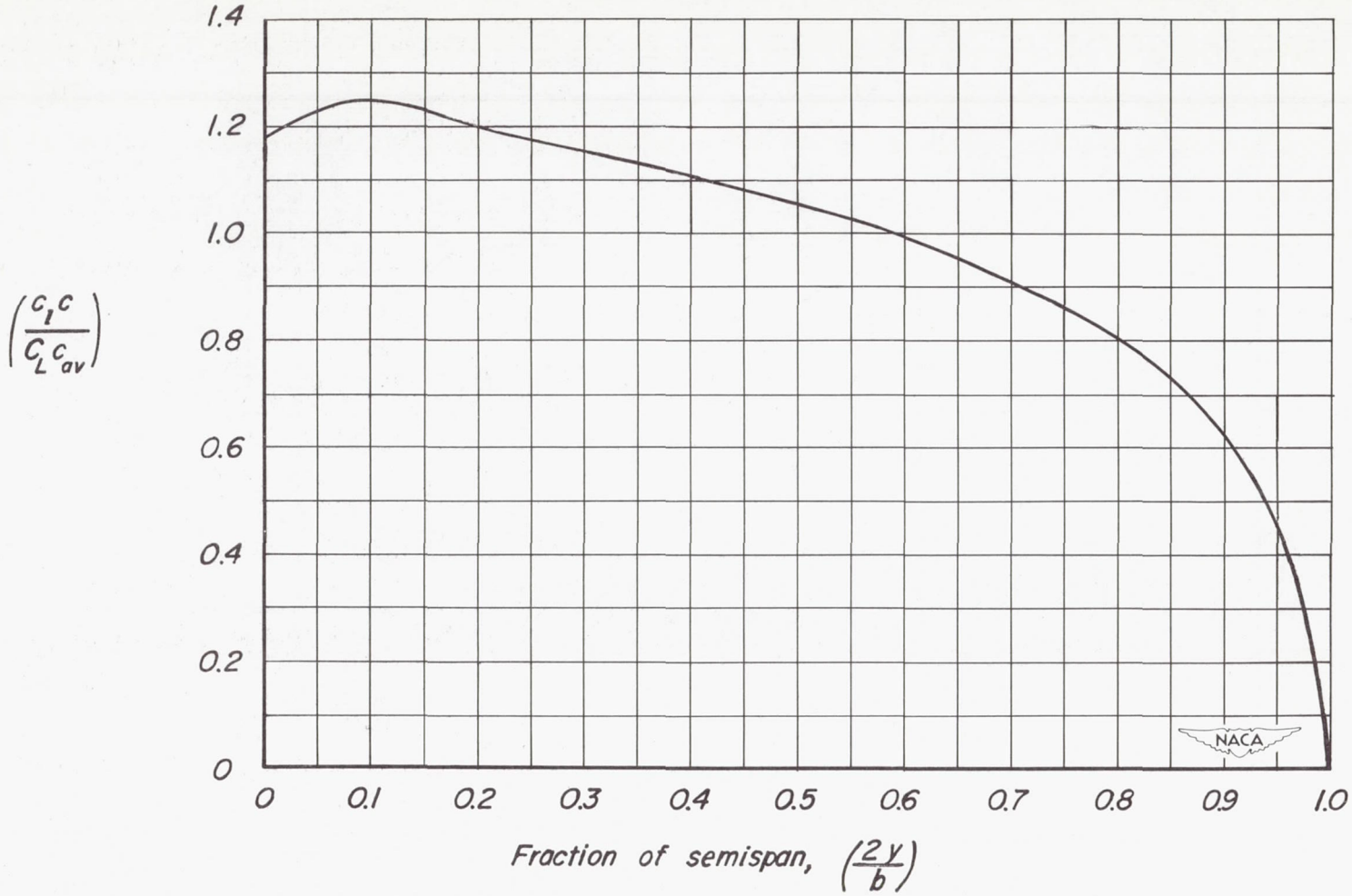

Figure 10.- Theoretical distribution of additional loading for wing and body combination as calculated by the method of references 12 and 13.

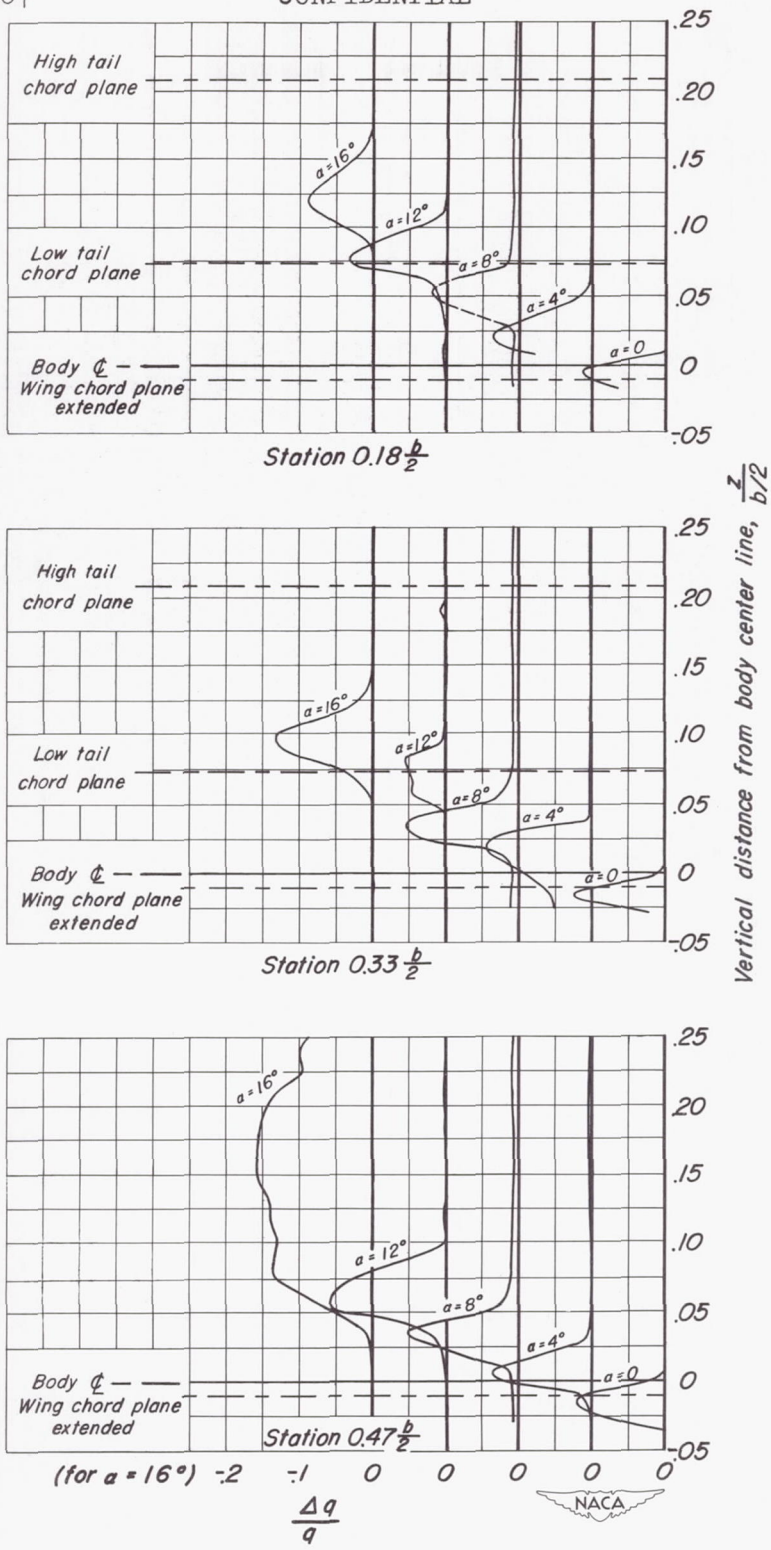

Figure 11.- Dynamic-pressure loss in the wing wake as a function of vertical distance from the body center line for several angles of attack and three spanwise stations at a Reynolds number of 11,000,000; M = 0.20.

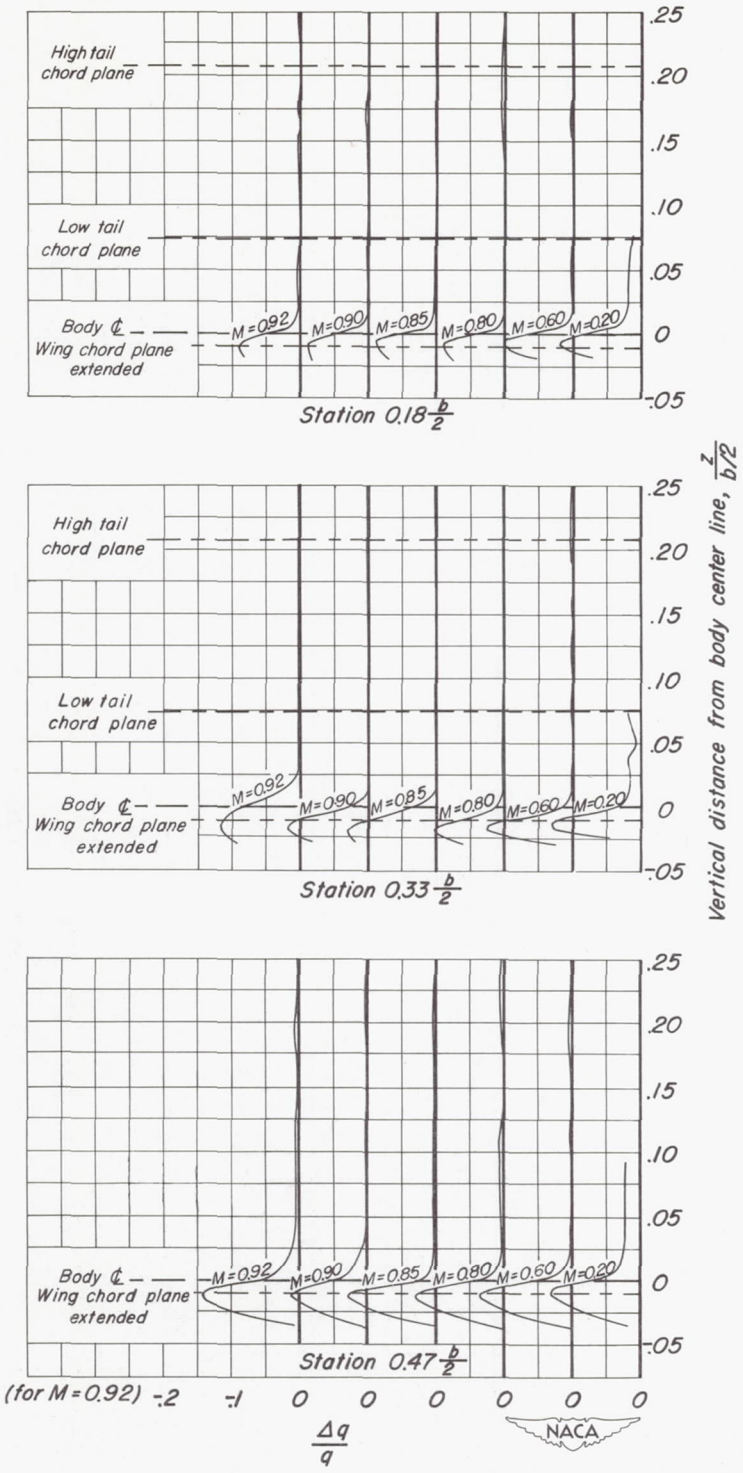

(a) $\alpha = 0^{\circ}$

Figure 12.- Dynamic-pressure loss in the wing wake as a function of vertical distance from the body center line for various Mach numbers and three spanwise stations; R = 2,000,000.

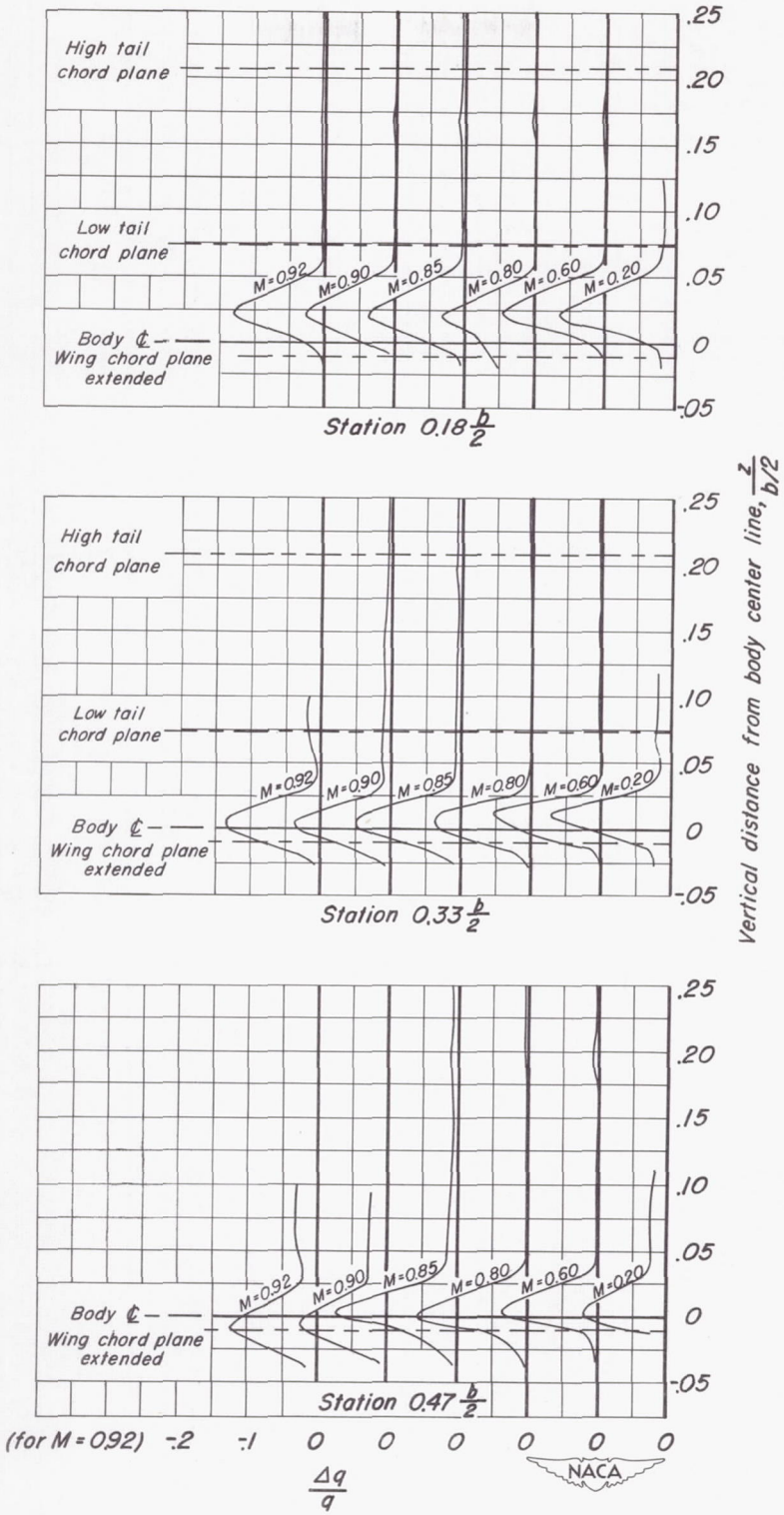

(b) $\alpha = 4^{\circ}$

Figure 12.- Continued.

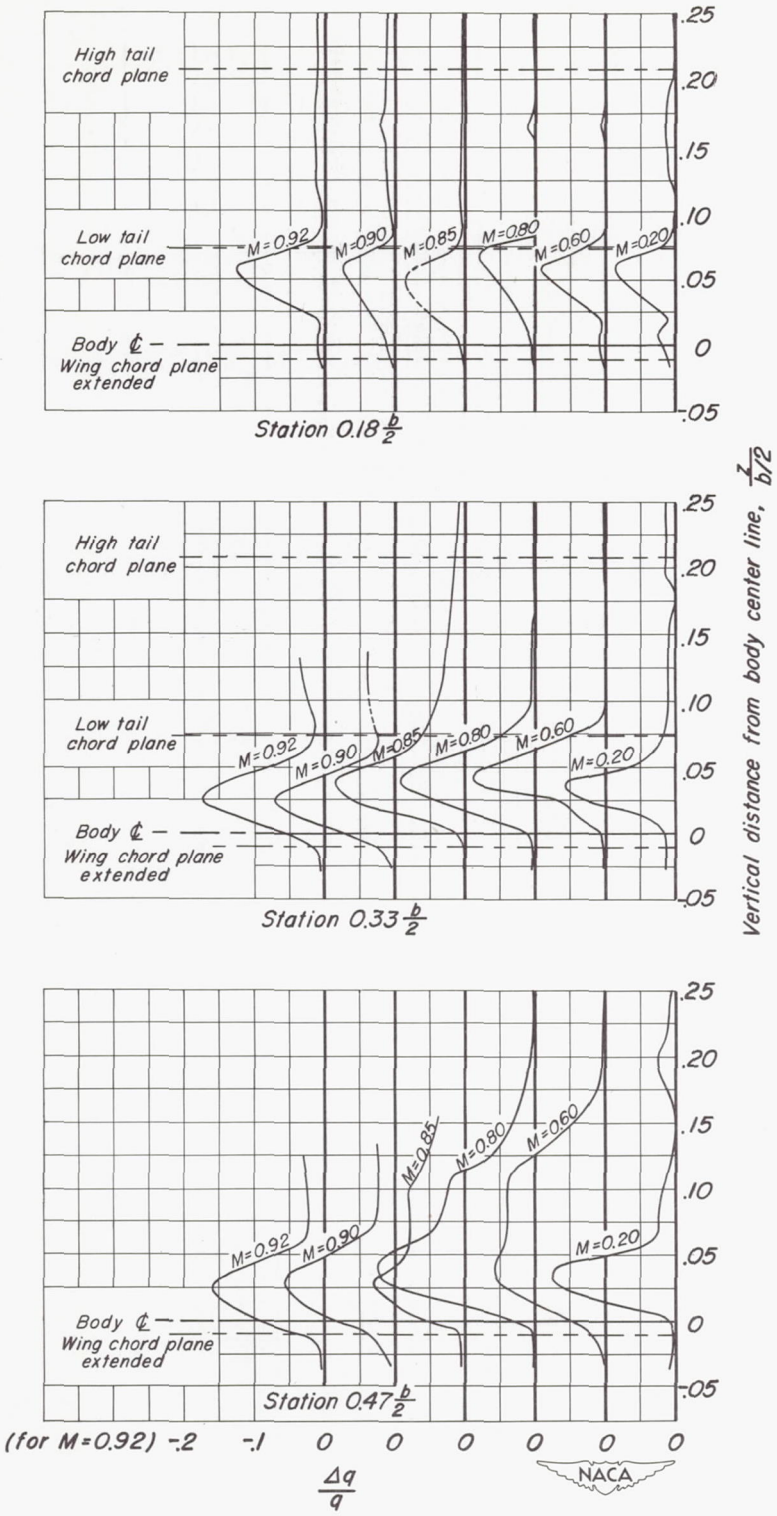

(c) $\alpha = 8^{\circ}$

Figure 12.- Continued.

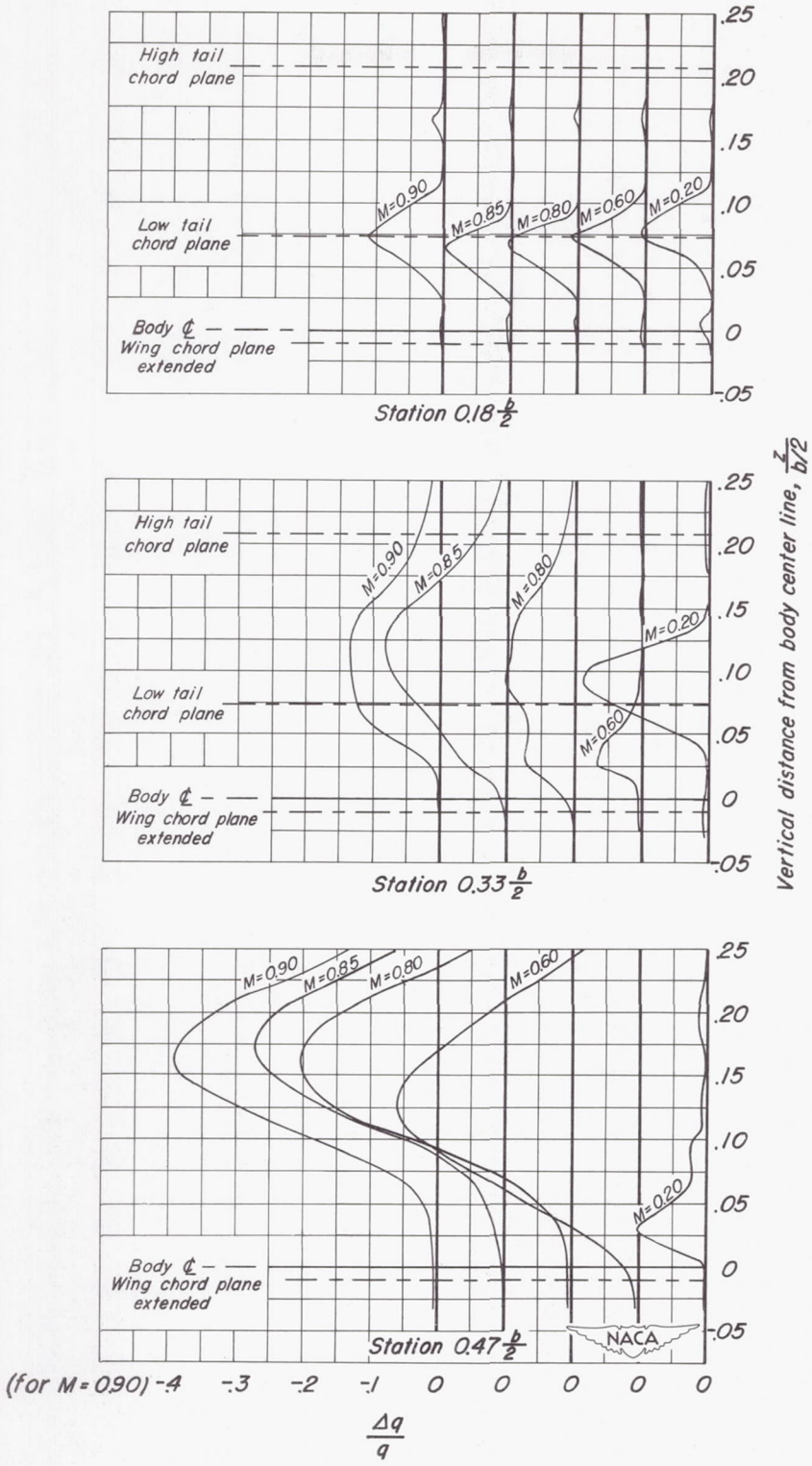

(d) $\alpha = 12^{\circ}$

Figure 12.- Continued.

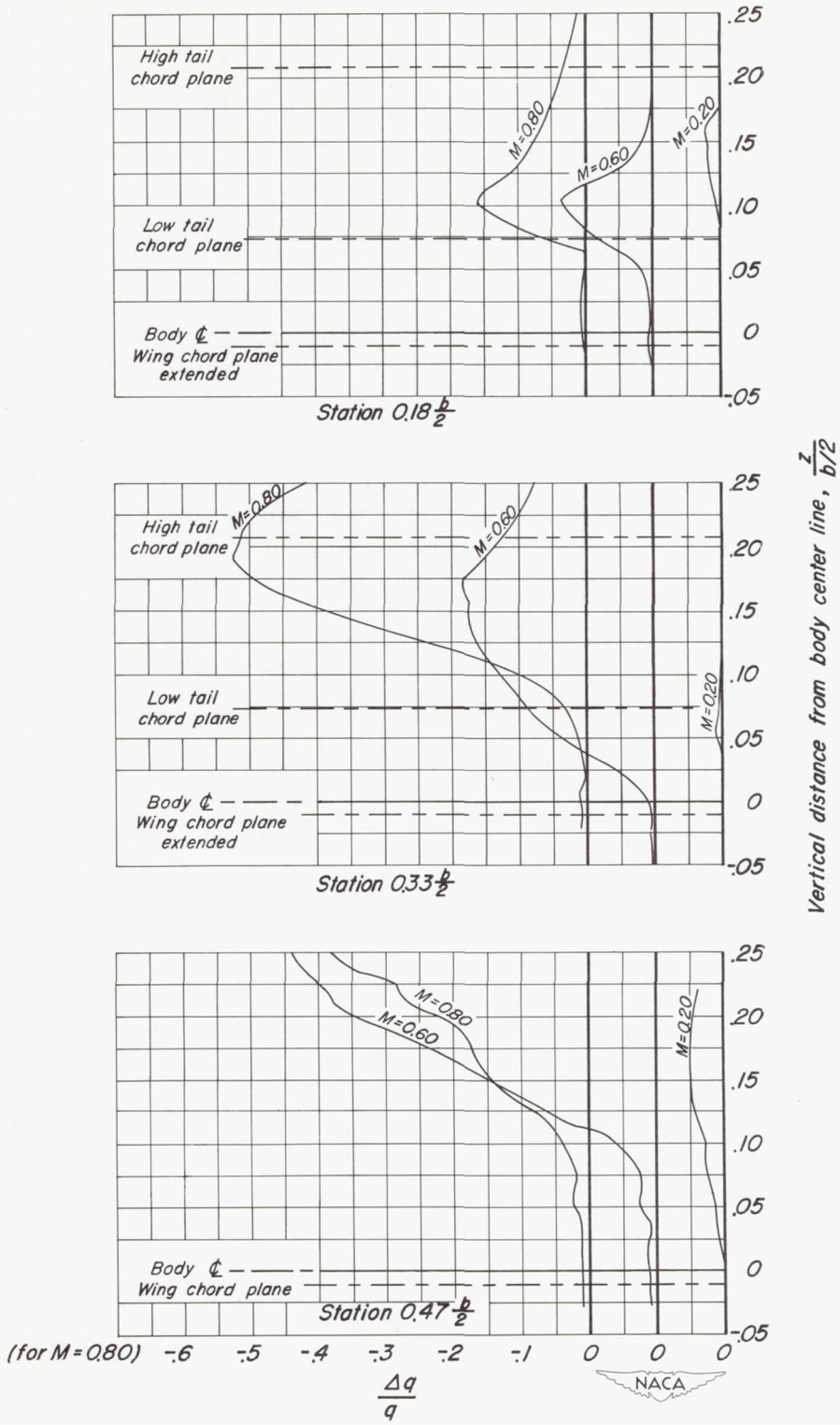

(e) $\alpha = 16^{\circ}$

Figure 12.- Concluded.

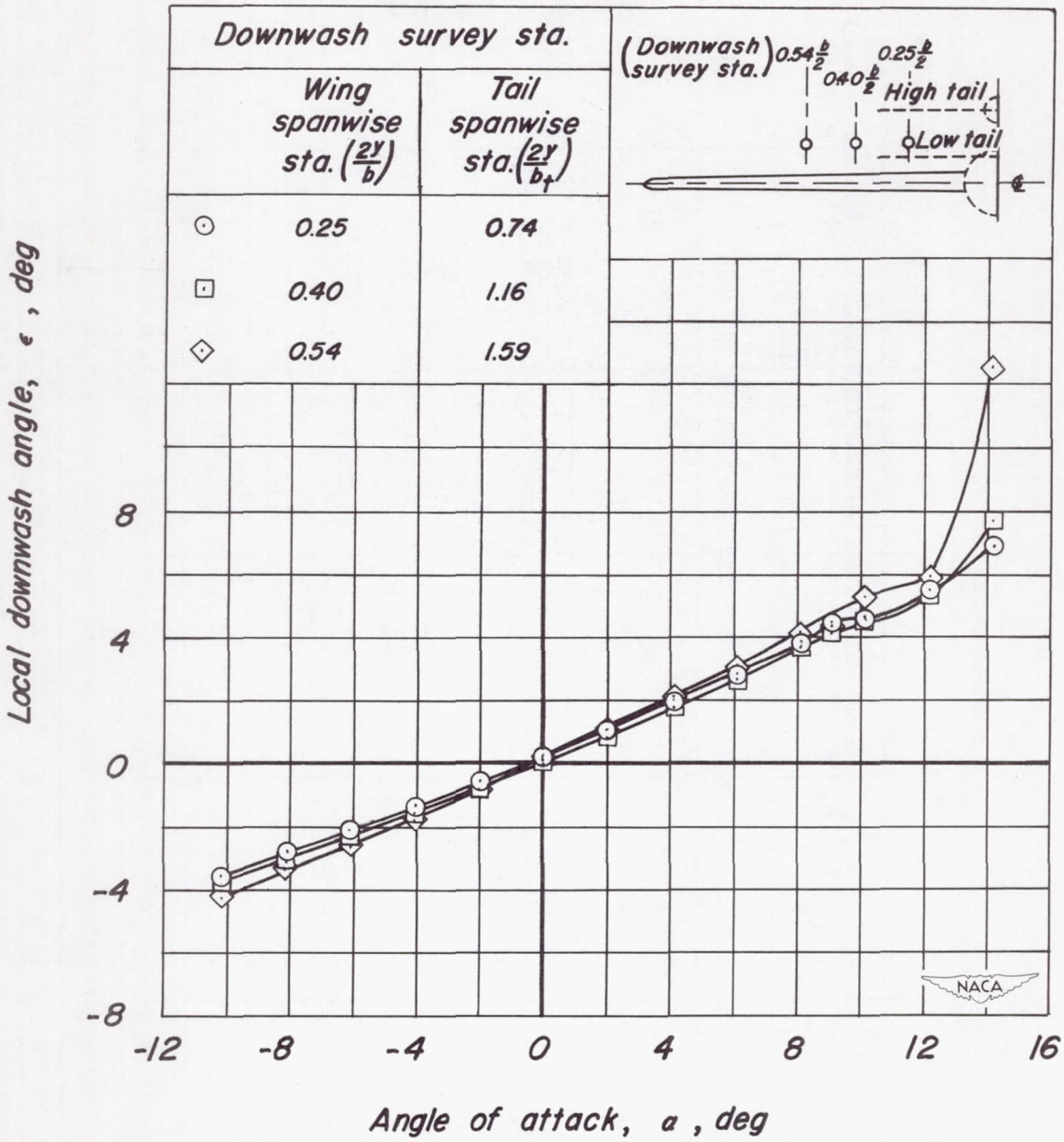

Figure 13.- The variation with angle of attack of the local downwash angle 0.12 b/2 above the wing chord plane extended at three spanwise stations and at a Reynolds number of 11,000,000; M = 0.20.

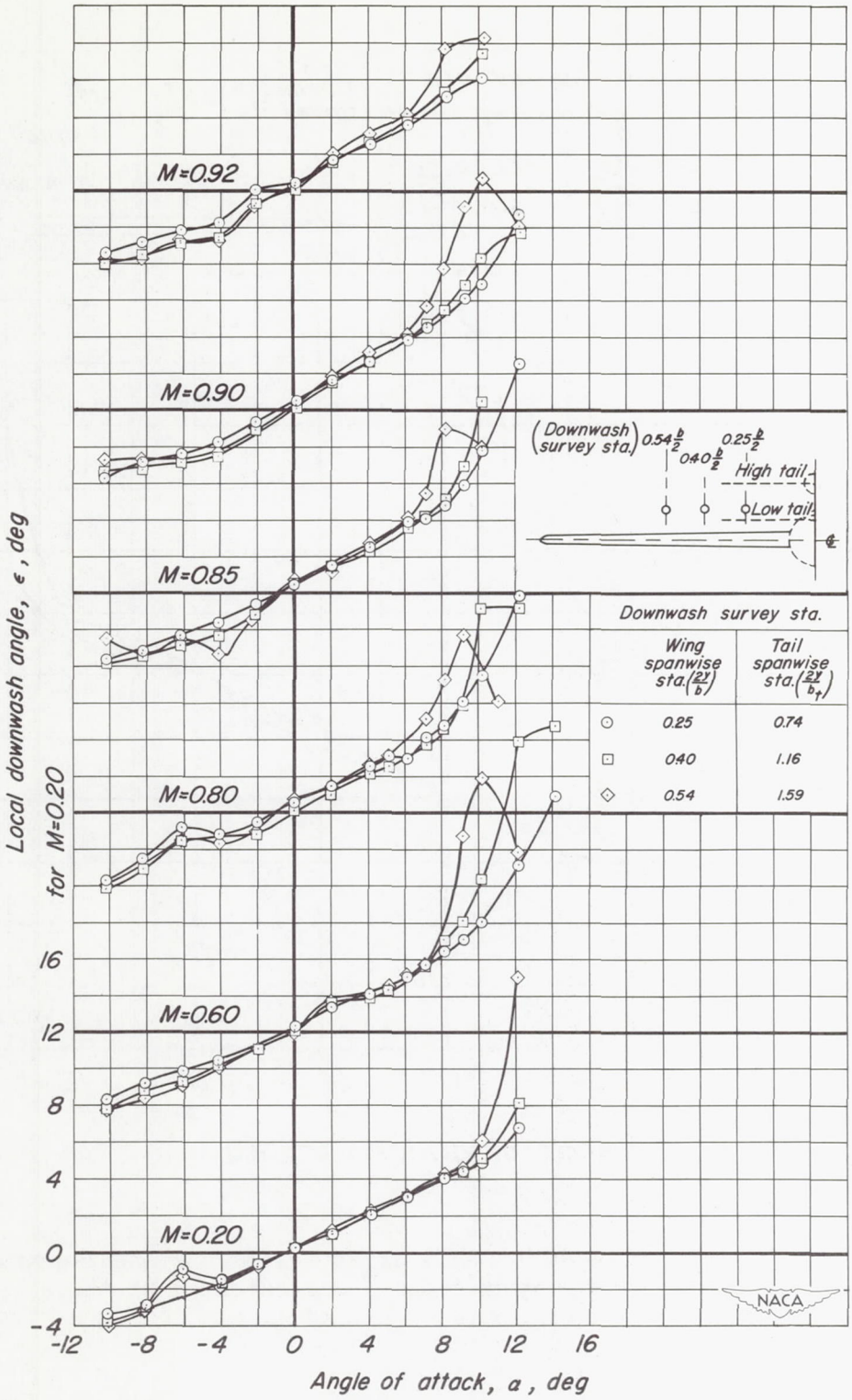

Figure 14.- The variation with angle of attack of the local downwash angle 0.12 b/2 above the wing chord plane extended at three spanwise stations and at various Mach numbers; R = 2,000,000.

CONFIDENTIAL

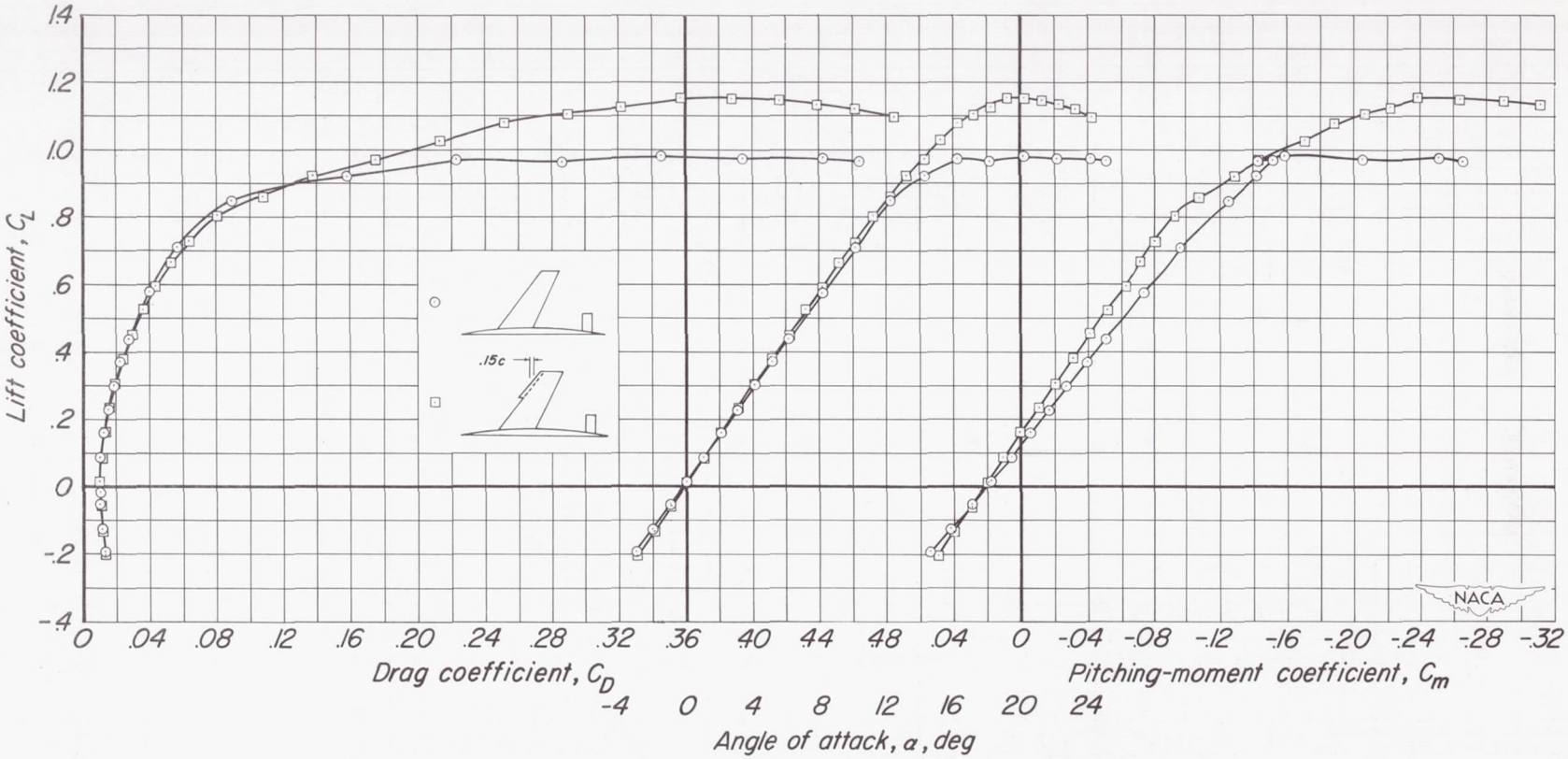

Figure 15.- The effect of a leading-edge extension on the aerodynamic characteristics of the model with the tail in the low position at a Reynolds number of 11,000,000; M = 0.20; $i_t = 0^{\circ}$.

CONFIDENTIAL

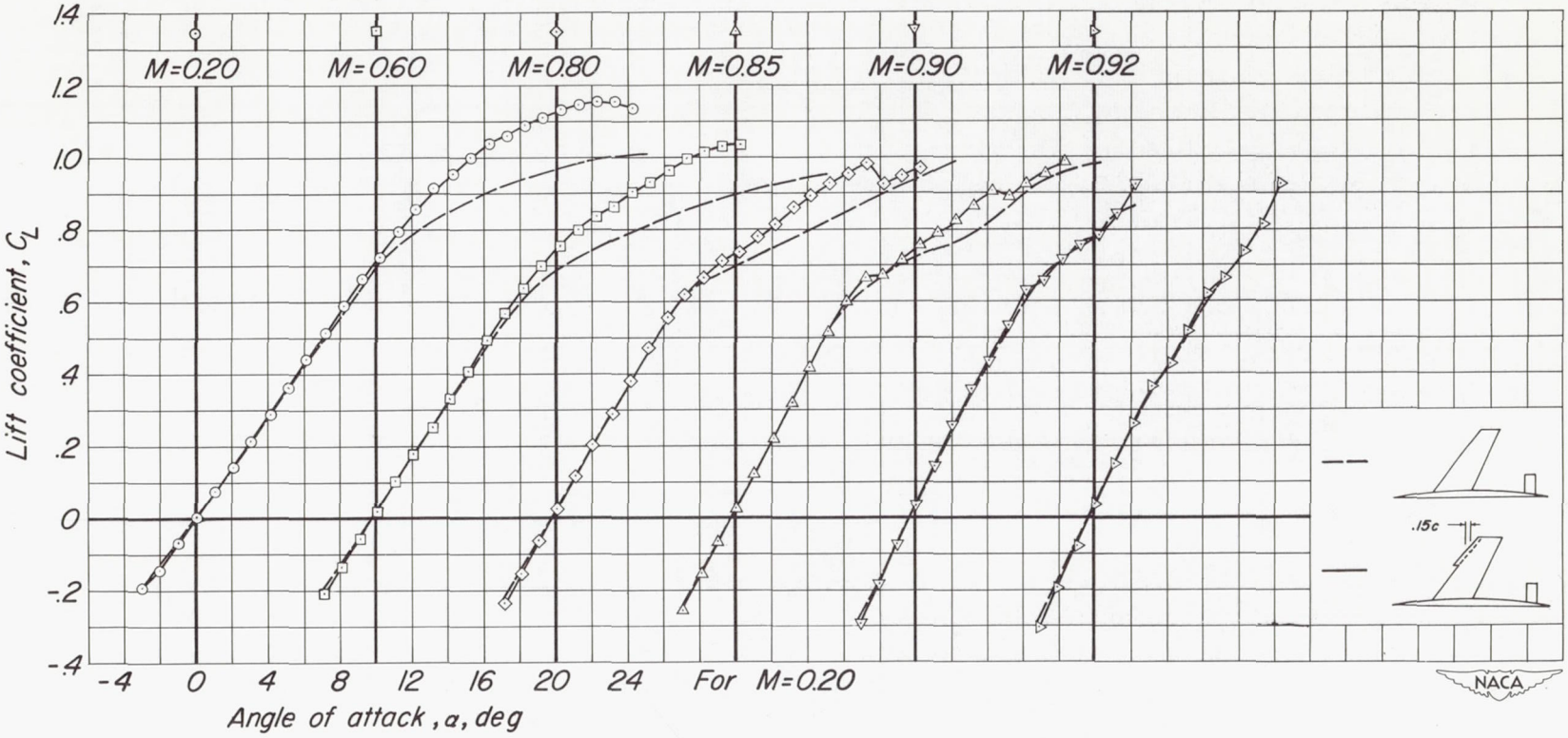

(a) C_L vs α

Figure 16.- The effect of a leading-edge extension on the aerodynamic characteristics of the model with the tail in the low position at various Mach numbers; R = 2,000,000; $i_t = 0^{\circ}$.

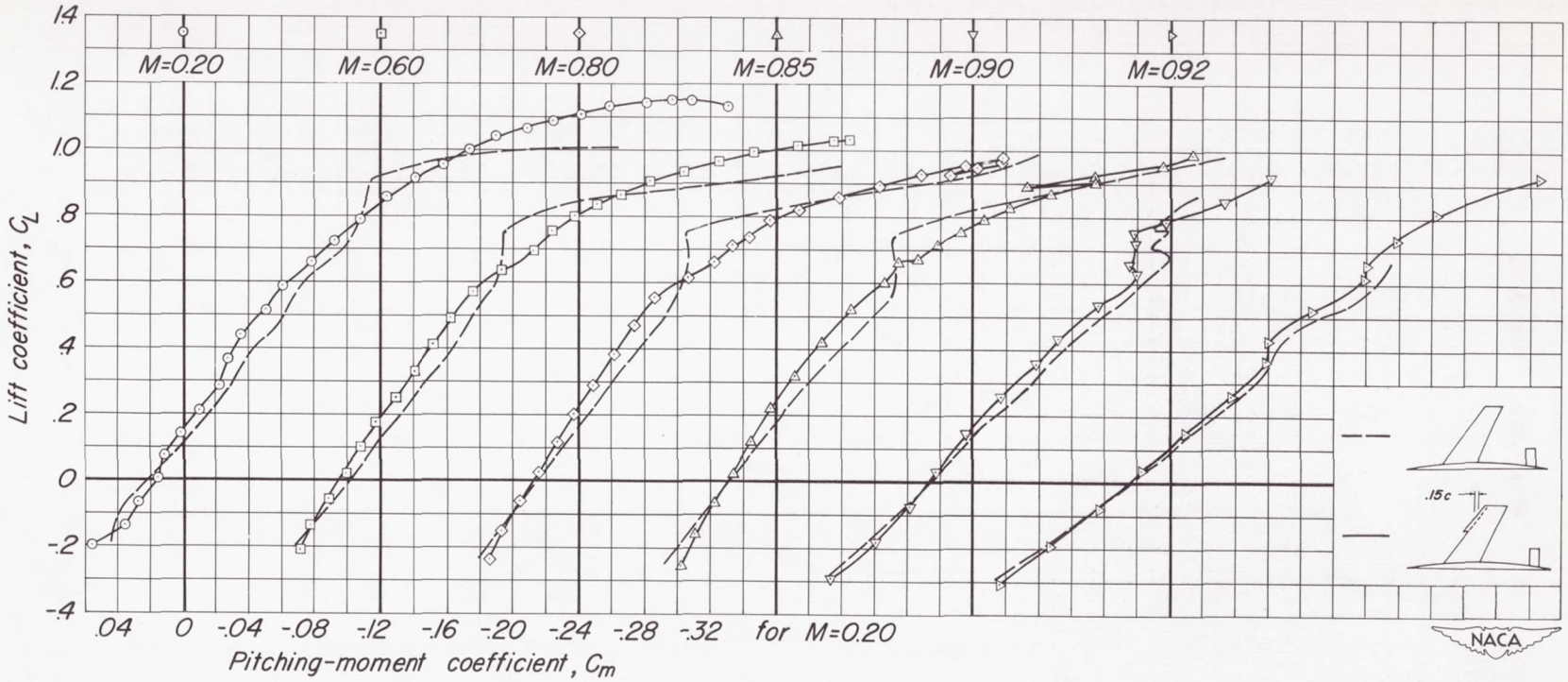

(b) C_L vs C_m

Figure 16.- Continued.

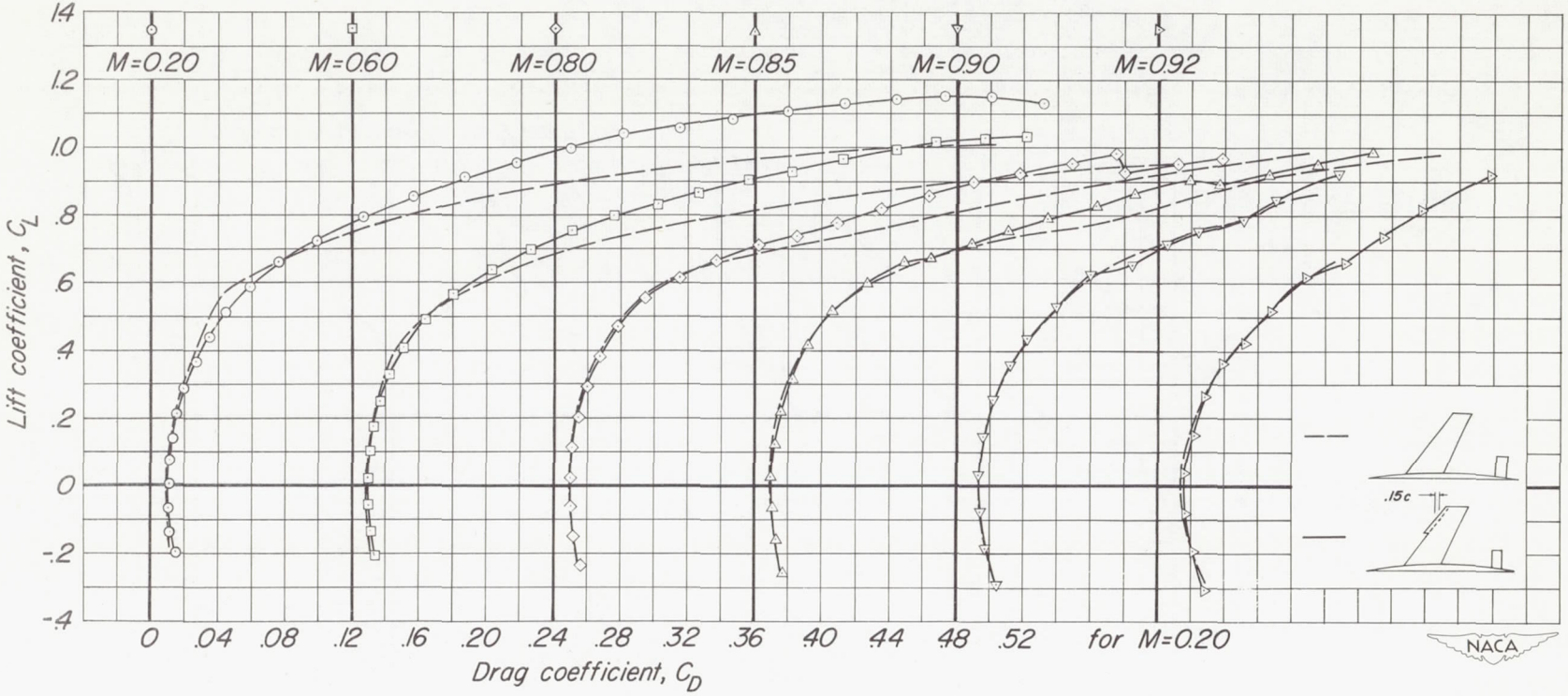

(c) C_L vs C_D

Figure 16.- Concluded.

NACA-Langley - 3-9-54 - 325

CONFIDENTIAL

CONFIDENTIAL